Offshore Wind Turbine Array

Kyle Beland, Jeremy Bibeau, Christopher Gagnon, Jacob Landry

Advisor: **Professor Martin Wosnik**

Graduate Student Co-Advisor: **Kyle Charmanski**

TECH 797 Ocean Projects

Final Report

This work is the result of research sponsored in part by the New Hampshire Sea Grant College Program through NOAA grant # NA10OAR4170082, and the UNH Marine Program.

Abstract

The goal of this research project was to systematically investigate how turbine spacing affects turbine and array power output, using small arrays of scaled model wind turbines. Realistically scaled models of 5MW offshore wind turbines were designed, fabricated and characterized with respect to performance. Wind turbine arrays of various configurations (e.g., arrays of 1xN, 1x9, 3x3 turbines) were then installed and tested in a high Reynolds number turbulent boundary layer in the UNH Flow Physics Facility. Turbine spacing was varied, power output, tip speed ratio and thrust of turbines were measured, and array power was correlated to array area. The data obtained can help improve the wind farm energy yield per unit cost, which is driven by a tradeoff between improved turbines spacing vs. increased cost due to larger ocean area used.

Table of Contents

List of Figures

List of Tables

Introduction

Large-scale deployments of renewable energy technologies are needed to address growing concerns about finite fossil fuel resources, and pressing environmental concerns about pollution and reduction of carbon dioxide (CO_2) . Wind energy is becoming more popular world-wide as it is one of the cleanest renewable power sources used today. In 2011, 2.9% of the United States electricity generation was from wind power. **[11]** However, there is a target of 20% of total U.S. electricity generation from wind energy by 2030 **[12]**.

Offshore wind farms locations have been more favorable than land-based farms due to ideal wind environments and availability of space in the open ocean. Offshore wind farms can also be placed within reasonable distance of load centers on the coasts of the United States. Depending on the location of the offshore wind turbine array, they can either be rigidly bottom-mounted or floating turbines. In shallow water often found near coastal regions, turbines are typically rigidly mounted to the sea floor. Cape Wind, off the coast of Cape Cod, Massachusetts, is the U.S.'s first development of an offshore wind farm and is currently in the beginning stages of construction. Many more offshore wind farms are in consideration and in the permitting stages so that the U.S. can reach its projected target to produce 20% of its electricity from wind by 2030.

The wind energy input throughout large wind farms tends to decrease due to wake effects from the leading turbines **[9]**. These array losses can be significant to onshore and offshore wind farms as today's wind farms are not reaching their maximum potential of power generation output due to improper array spacing. The wind velocity deficit behind the leading turbine can build up as it traverses through the turbine array leaving the trailing turbines less effective, which, in turn, could hinder potential profits per year. The typical loss a wind turbine array could encounter can be from 5% to over 15% depending on the array layout. **[2]**

The objective of this research project was to use small arrays of realistically scaled model wind turbines to systematically investigate how turbine spacing affects turbine and array power output. The goal was to better understand how neighboring turbine wakes influence each other, to improve the turbine spacing and the wind farm energy yield per unit cost, which is driven by ocean or land area used.

Previous studies analyzed the influence of the incoming wind flow on turbine performance and turbine wake. In 1992, Sheinman and Rosen found that neglecting the effect of turbulence in the incoming flow can cause an overestimation of 10% of the turbine output **[3]**. Medici and Alfredsson, 2006, performed a wind tunnel study where the wake of a model turbine was found to be noticeably changed depending on how much turbulence was present in the oncoming flow **[4]**. From this it can be expected that more significant differences in the dynamics of the wake can be seen if the turbine was placed within a turbulent boundary layer, such as the atmospheric boundary layer

In the present study, the goal is to systematically investigate the power output of an offshore wind turbine array for variable turbine spacing. Realistic scale models of 5MW offshore wind turbines were designed, fabricated and characterized with respect to performance. Wind turbine arrays of various configurations (e.g. 1xN, 1x9, 3x3) were then installed and tested in a high Reynolds number turbulent boundary layer in the UNH Flow Physics Facility (FPF). Turbine spacing was varied, power output and thrust of turbines was measured, correlating array power to array area.

Research Approach

The goal of this study was to determine the efficiencies of various offshore wind turbine arrays. The spacings of the turbines were varied in the spanwise and streamwise directions. The output power of each turbine was recorded to determine the total power output and hence the efficiency of each array. A thorough analysis of similar studies and actual turbines helped derive a scale for the turbines used in the current study while staying within the physical constraints of the boundary layer developed in the Flow Physics Facility.

First, the model turbines must be designed and fabricated. The blades were designed using 1-dimensional blade momentum theory. When using the 1-dimensional blade element momentum theory the design tip speed ratio, number of blades, design wind speed, and turbine diameter must be chosen. Pitot static tubes were used to determine the wind speed in the wind tunnel seen by the model turbines.

The axial force (thrust) acting on the turbine rotor is an important parameter to measure. The force acting on the turbines was then used to calculate the thrust (drag) coefficient, defined with the area swept by the rotor. The force will be measured by placing one of the nine turbines on a custom force balance.

The power generated by the turbines was also measured in the study. This was accomplished by attaching the turbines to 24 volt three-phase motors and running them as generators. The power generated by the turbine was determined by measuring voltage and current output of the motor. Angular speed of the motor was also found through the output of the motor. This was accomplished by performing a Fast Fourier Transform (FFT) of the output voltage of the motor to find the frequency the motor was rotating at.

Upon completion of the model turbine fabrication the testing process can ensue. A test plan was followed for all studies that were completed [see appendix].

Scaling

An important aspect of this study was the scaling of the wind turbines to obtain realistic model wind turbines. To properly scale down large scale wind turbines to a workable model size that can be used in available test facilities, three non-dimensional parameters need to be considered. These are:

- coefficient of performance (C_p), defined as $c_p = \frac{P}{\frac{1}{2}\rho A U^3}$
- coefficient of thrust (C_t), defined $C_t = \frac{F_t}{.5\rho A U^2}$
- and tip speed ratio (TSR), defined as$TSR = \frac{\Omega R}{U_\infty}$

To determine appropriate values for these coefficients, information from actual full size wind turbines was used.

A scale was chosen to ensure all parameters in the study scale appropriately to the full-scale turbines being studied. Several full-scale offshore wind turbines were examined. The two parameters of focus are the hub height and the rotor diameter. These parameters can be seen in Table 1 for multiple turbines. In this study a 5 MW turbine with a rotor diameter of 125 m is being scaled down by a factor of 500 resulting in a model rotor diameter of 25 cm. The hub heights of offshore wind turbines can have a varying range, they are commonly lower than that of onshore wind due to the difference in wind conditions for onshore and offshore. This is due to there being a less disturbed flow over the ocean caused by lack of obstruction commonly seen on land such as trees, hills, and mountains. For this study, a hub height that is average of offshore wind turbines was chosen to be 75% of the rotor diameter. The hub height this corresponds to for this study is 18.75 cm. This hub height placed the total turbine height in the bottom quarter of the boundary layer in the University of New Hampshire's Flow Physics Facility (FPF).

Table 1: Specifications of select offshore wind turbines

	Rated Power (MW)	**Rotor Diameter (m)**	**Hub Height (m)**
Vestas V80	2	80	60-100
SWT-3.6-107	3.6	111	87
Repower-5M	5	126	85-95
SWT-6.0-154	6	154	Site Specific

Experimental Facilities

Small (Student) Wind Tunnel

The initial model wind turbine development work and free stream testing was performed using a small wind tunnel in Kingsbury Hall located on University of New Hampshire's campus. The "student wind tunnel" is the 404 modified model manufactured by Engineering Laboratory Design (ELD), Inc. The wind tunnel is an Eiffel type, open circuit wind tunnel, which draws air through a honeycomb and screen pack inlet and is accelerated through the contraction leading into the test section. The system air then recovers static pressure as it passed through a diffuser. The wind tunnel uses a cent-axial type fan powered by a 40 HP variable speed, DC Reliance motor and controller. The interior dimensions of the test section are 36"x18"x18" (LxWxH), and speeds from 2 m/s to 65 m/s can be reached. The test section of the student wind tunnel is fitted with 3/4" thickness, clear, GM grade, acrylic plexiglass to allow for a safe viewing area. The student wind tunnel is shown in Figure 1**.**

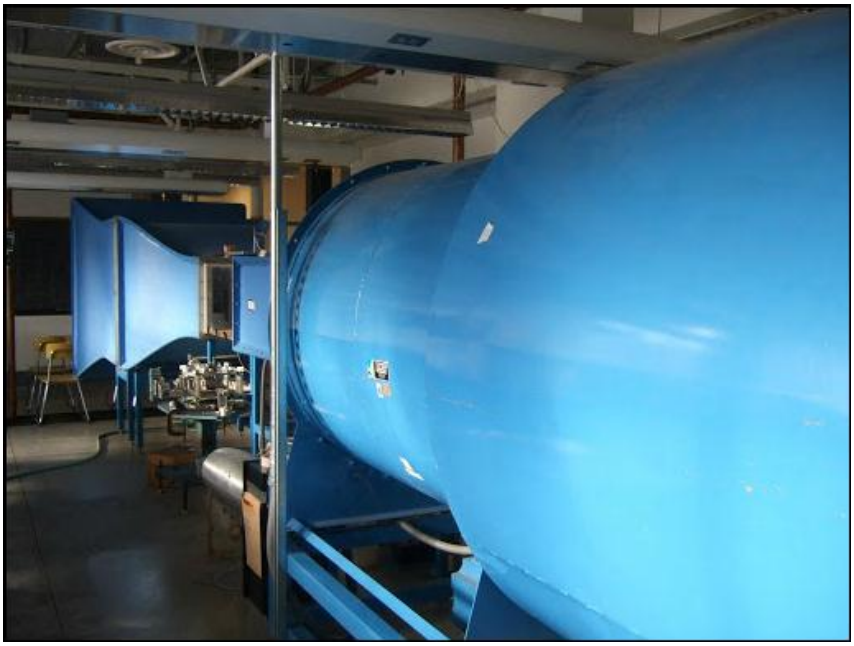

Figure 1: The ELD 404c Eiffel-type "Student Wind Tunnel" located in Kingsbury Hall, with test section dimensions W 18" x H 18" x L36",

The student wind tunnel is adequately equipped with the measurement systems required to record the data that was desired, both wind velocity and drag. A list of the equipment for free stream testing can be found in Table 2.

Table 2: Equipment used to conduct free stream experiments.

Pressure Measurement	
	20 Tube Manometer
	Static and Stagnation Pitot Tubes
Force Measurement	
	The Golden Standard Load Cell
	TQ AFA2 Single Component Lift and Drag Balance
Miscellaneous	
	Multi-meter

Flow Physics Facility

Measurements of the performance of individual wind turbines and wind turbines arrays in a turbulent boundary layer were conducted in the UNH Flow Physics Facility (FPF). The FPF is the world's largest flow-physics quality turbulent boundary layer wind tunnel. The test section measures 72 m x 6 m x 2.7 m (LxWxH), The FPF is an open return type tunnel driven by two 400-horsepower fans. The maximum test section velocity in the facility's present configuration is 14 m/s. The FPF is shown in Figure 2

Figure 2: The UNH Flow Physics Facility, with test section dimensions W 6.0 m x H 2.7 m x L 72 m.

The FPF is adequately equipped with measurement, traversing, and data acquisition systems. A complete list of the equipment can be found in the appendix. The equipment used for the boundary layer and array section of this study can be seen in Table 3

Table 3: Equipment used to conduct boundary layer and array experiments with model wind turbines.

Pressure Measurement	
	MKS Type 690A 10 Torr (1.33 kPa) Max Differential High Accuracy Pressure Transducer
Data Acquisition System	
	National Instruments NI-PXI-1042 Computer
	BNC-2120 Multifunction DAQ Board
Miscellaneous	
	Tektronix TDS2004B 4- Channel Digital Oscilloscope Fluke 97 Hand Held Scope

The test section is equipped with several drag plates. Each drag plate covers a pool which measures 2 m x 2 m x .15 m.

The extremely long test section of the FPF allows for the natural growth of very thick boundary layers. The theoretical boundary layer height for a turbulent flow over a flat plate is given by

$$\delta \approx 0.372 {Re_x}^{-1/5} \tag{1}$$

where Re_x is the Reynolds number as a function of downstream distance **[7]**. Using Equation **(1)**, the theoretical boundary layer height as a function of free stream velocity and downstream distance is shown in Figure 3

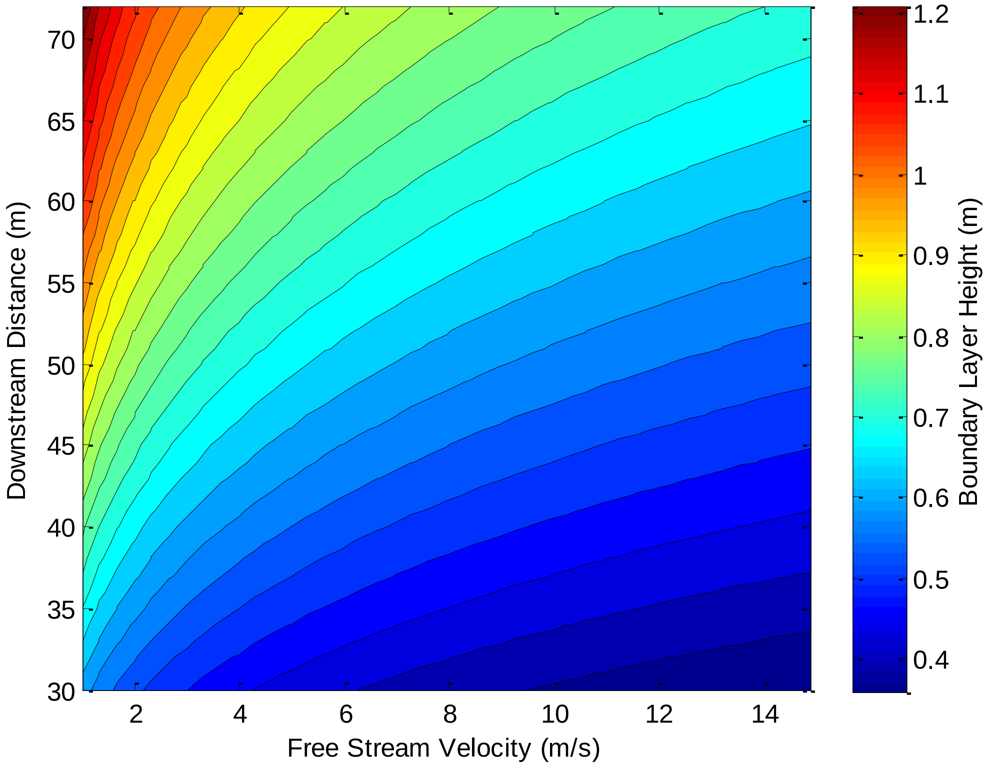

Figure 3: Theoretical boundary layer height for a turbulent boundary layer as a function of downstream distance and free stream velocity **[7]**.

Model Turbine Blades

Theory

Blade Design

The scaled turbine was designed using Blade Element Momentum (BEM) Theory, the same approach used to design wind turbine rotors in the wind energy industry **[8]**. Using a specified rotor radius (for our initial design case r = .125m) the blade was first discretized into 12 finite pieces. Each element has its own angle of attack, pitch, wind angle, and angular velocity. A diagram of this is shown in Figure 4.

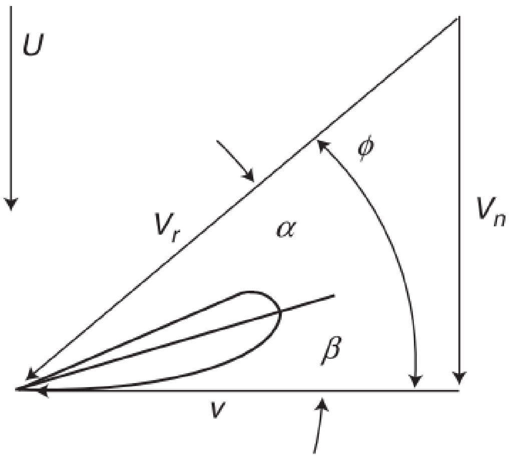

Figure 4: Diagram of blade element parameters.

As shown in Figure 4, each blade element experiences a relative velocity vector which is a function of the free stream wind velocity and tangential velocity of the blade. The angle the relative velocity makes with the chord line of the blade element is defined as the angle of attack, α. The angle between the relative wind vector and the tangential velocity vector is known as the relative wind angle, φ. The difference between φ and α is known as the section twist angle. Each element also has its own local speed ratio, defined as

$$x = (r/R)\lambda\,, \tag{2}$$

where r is the local radius of the element, R is the overall radius of the blade, and λ is the target tip speed ratio of the turbine. For the initial blade design, a target tip speed ratio of seven was used. This tip speed ratio is well within the normal range of tip speed ratio for full scale turbines. The coefficient of performance for the blade is computed by

$$C_{p,i} = \frac{8\Delta x}{\lambda^2} sin^2\phi_i(cos\phi_i - xsin\phi_i)\ (sin\phi_i + xcos\phi_i)(1 - \frac{C_d}{C_l}cot\phi_i)x^2, \tag{3}$$

where φ_i is the local relative wind angle, Δx is the change in local speed ratio (a constant), C_d is the drag coefficient, and C_l is the lift coefficient. It is important to note, C_d and C_l are functions of the airfoil chosen, angle of attack, tip speed ratio, and wind speed. The lift and drag data for this design process was collected from empirical results. The relative wind angle, φ, was computed by

$$\varphi = tan^{-1}\frac{2}{3x}, \tag{4}$$

As this array of values is only a function of tip speed ratio and blade length, the only selectable parameter is the angle of attack. A Matlab script was written to run through each angle of attack for which empirical data was available and find the most efficient rotor design. Using the parameters of the most efficient design, the chord length of each blade element was computed by

$$\mathrm{c} = \frac{8\pi r sin\varphi}{3BC_l x}, \tag{5}$$

where B is the number of blades in the design. It is important to note, the lift coefficient used is pulled from the empirical data for the most efficient angle of attack found using the Matlab script. The script outputs an array of twist angles and chord lengths which are imported to SolidWorks where the blade is modeled.

Power Extraction

In order to calculate power extraction of the motor, the following equation can be used,

$$P = T * \omega \tag{6}$$

Where P is the power extracted, ω is the angular velocity and torque T represents the torque of the motor. For the 12V DC Pittman motor, the torque of the motor was determined using the voltage-RPM plot in Figure 5.

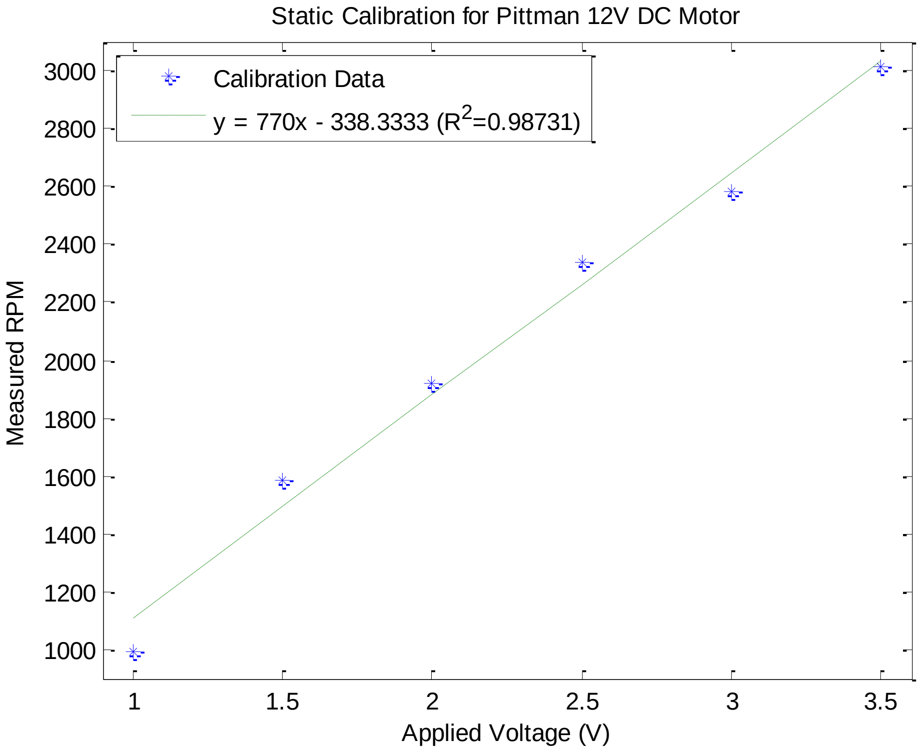

Figure 5: Voltage vs. RPM for 12V DC Pittman motor with blades attached.

The slope of the linear line represents the voltage constant (K_V) of the motor which can then be converted to the torque constant (K_T) using the following equation,

$$K_T\left(\frac{lb*in}{amp}\right) = 15.3 * K_V\left(\frac{V}{\frac{rad}{sec}}\right). \tag{7}$$

For the 24V motor, the torque constant provided by Anaheim Automation was used. The motor torque constant is used in the following equation to calculate torque,

$$T = K_T * I \tag{8}$$

where "I" is the current in the series circuit setup. A tachometer was used to determine the angular velocity (ω) of the blades at different voltages of the motor. With a known torque constant the power curve of the blades can now be determined using equations (8) and (6) for every measured angular velocity and amperage using the tachometer and multi-meter respectfully. In order to gain accurate data points of the power curve a potentiometer was connected into the series circuit and adjusted accordingly, altering the angular velocity and current. Using the power computed using Equation 2, the coefficient of performance was computed using

$$C_p = \frac{P}{\frac{1}{2}\rho A U^3} \tag{9}$$

where ρ is the density of air, A is the swept area of the blades, and U is the free stream wind speed.

Experimental Procedure

Characterization of the blades designed using 1-D Blade Element Momentum Theory was performed in the University of New Hampshire Mechanical Engineering Student Wind Tunnel. To begin, the designed blade, hub and nose cone assembly were attached to the testing motor and mounted on a sting which was in turn connected to the force balance in the student wind tunnel. Characterization was achieved by connecting a potentiometer with a resistance range of $100\ \Omega - 0\ \Omega$ in series with the testing motor and measuring the current across it that was generated by the motor.

To begin testing, the student wind tunnel was set to a wind velocity of approximately $7\frac{m}{s}$. While that velocity was held constant the resistance of the potentiometer was slowly decreased, resulting in the rotor decreasing in speed. Three different measurements were taken for each setting of the potentiometer. The current over the potentiometer was recorded at various resistances, pitot tube measurements were recorded to calculate wind tunnel velocities, and angular speed of the blades were recorded using a light strobe tachometer. This procedure was completed at each turn of the potentiometer. At each position of the potentiometer the drag force acting on the rotor was also recorded. All of this data was recorded for later analysis.

Results and Discussion

Using blade element momentum theory, and the Matlab script previously described, an initial blade design was developed by first choosing the airfoil type, NACA 2412, a tip speed ratio of 7, and a diameter of 0.25m. The total twist angle consisting of section twist and angle of attack, and chord length outputted by the Matlab script can be seen in Table 4.

Table 4: Blade design 1 characteristics

r/R	**Twist Angle** (°)	**Chord Length** (m)
0.083	60.0	0.0572
0.17	39.2	0.0572
0.25	26.3	0.0401
0.33	19.2	0.0298
0.42	14.9	0.0233
0.5	12.2	0.0191
0.58	10.2	0.0161
0.67	8.8	0.0139
0.75	7.7	0.0122
0.83	6.9	0.0109
0.92	6.2	0.0098
01	5.7	0.0089

The blades and hub with the specifications shown in Table 4 were printed in ABS plastic and took roughly 9 hours to print the entire assembly. The finished blades and hub assembly can be seen in Figure 6.

Figure 6: Blade design 1 and hub assembly

The blades and hub assembly shown in Figure 6 were mounted to a12 V DC Pittman motor. The blades were then subjected to various winds speeds in the Student ME Wind Tunnel, while collecting drag force and power data. The drag data can be seen in Figure 7.

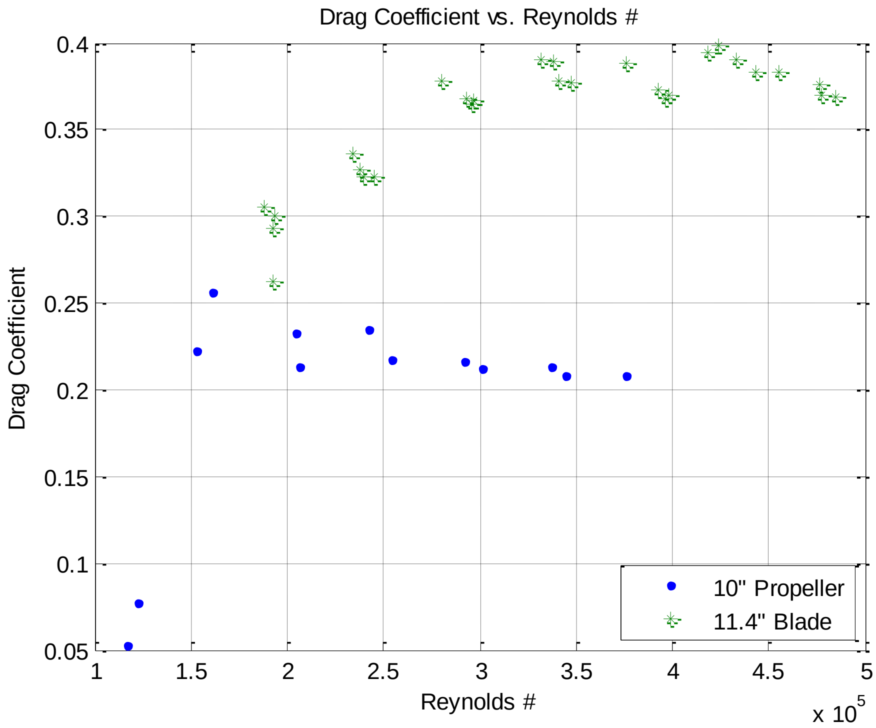

Figure 7: Drag coefficients vs. Reynolds number for blade design 1 and model airplane propeller.

As shown in Figure 7, the designed blades have a significantly higher drag coefficient than a model plane propeller that was tested for comparison. The comparison to the RC airplane propeller is meant to serve only as a general evaluation of the blades performance. Note that the airplane propeller cannot be used as a wind turbine rotor, even when turned around, since the camber of the foils is on the wrong orientation. This comparison indicates further increases in drag coefficient would be possible with continued development in new blade designs.

Using the motor current output of the 12V DC Pittman motor, measured angular velocity, and pitot-static tube measurements, it was possible determine the relationship between the power coefficient and TSR for the first blade design. The plot can be seen in Figure 8.

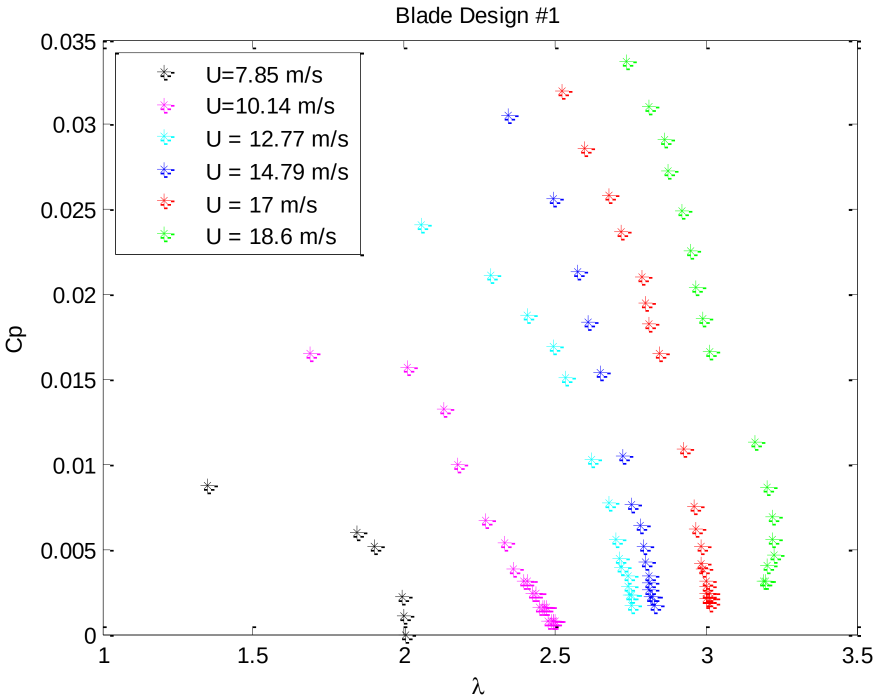

Figure 8: Coefficient of power vs. TSR using 12V DC Pittman Motor

The power coefficient data shown in Figure 8 indicates the peak efficiency for each speed was not reached during testing. This was believed to be a result of power output limitations of the 12V DC Pittman motor. To attempt to find the maximum efficiency of the designed blades, a new motor was purchased that was believed to be able to reach a high enough power output at the speeds blade design 1 would reach. It is important to note, due to the dimensions of the test section, the data was corrected for blockage effects. The velocity measurements taken were adjusted using

$$V_{corr} = V_o(1 + .25\frac{A_{obj}}{A_{test}}) , \qquad (10)$$

where V_o is the un-corrected velocity, A_{obj} is the area of the object being tested, and A_{test} is the cross sectional area of the test section. The specifications of the new motor are shown in Table 5.

Table 5: Specifications of the BLY172S-24V-4000 motor purchased through Anaheim Automation.

Rated Voltage	Rated Speed	Rated Power	Torque Constant	Voltage Constant
24 V	4000 RPM	30 W	5 ozf-in/A	3.72 V/kRPM

The procedure to find the power coefficient versus tip speed ratio for the initial blade design was run again using the new motor and the results can be seen below in Figure 9

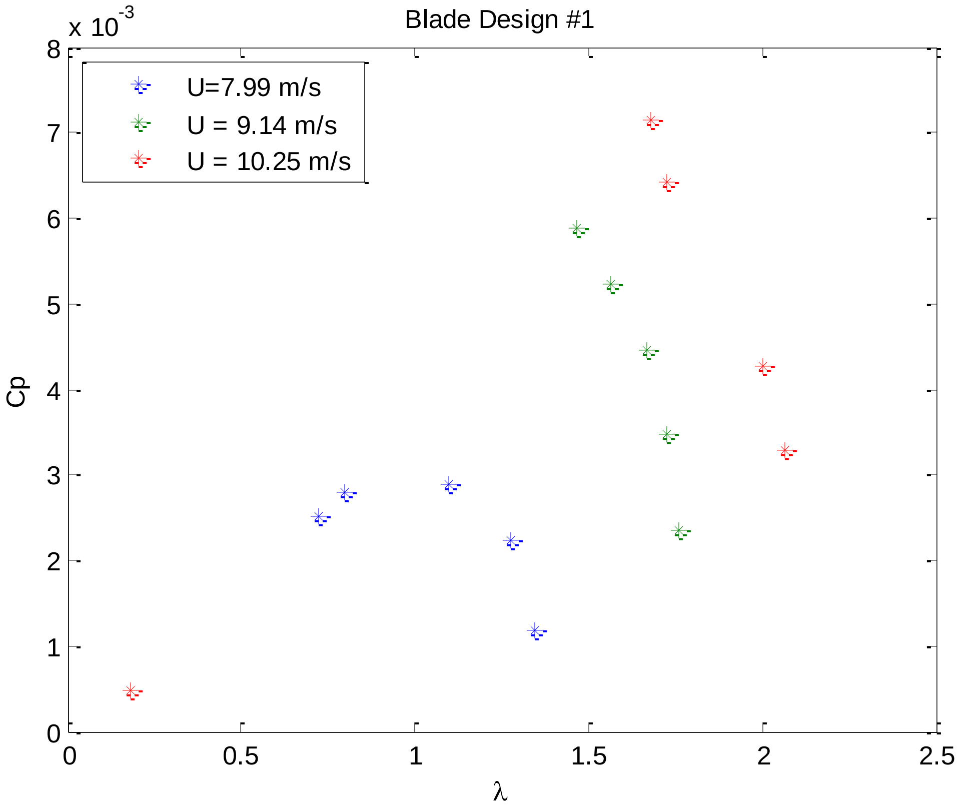

Figure 9: Coefficient of power vs. TSR for blade design #1 using 24VAnaheim Automation motor

It is clear from Figure 9 that the initial blade design does not reach the designed tip speed ratio. Although, the figure does show that the entire power curve of the blades can be captured using the new motor. Most importantly, the above figure shows how inefficient the first blade design was. It was clear the process of designing blades had not been perfected yet.

While a new blade design was being designed using the BEM theory and the Matlab script previously described was being fixed, an intermediate blade was modeled within SolidWorks, and 3-D printed in ABS Plastic. The design chosen was one modeled by Medici in a study of wind turbine wakes [2]. The purpose of using this design was to be able to continue to test the new 24V motor to verify that a more efficient blade design would not be limited by the new motor.

Table 6: Blade design 2 characteristics

r/R	**Twist Angle** (°)	**Chord Length** (m)
.25	15	.032
.5	35	.035
.75	31	.031
1	25	.025

The blade 2 design characteristics seen in Table 6 were modeled within solidworks, and 3-D printed in ABS plastic usign the University of New Hamphsire rapid protyper. The blade 2 and hub assembly can be seen in Figure 10.

Figure 10: Blade design 2 and hub assembly

The blade design in Figure 10 was attached to the 24V Anaheim Automation motor and run through a varying wind speed along with a varing resistance in the UNH Student Wind Tunnel. Drag, power, and flow measurement were recorded to analyze the blade design. In Figure 11 the drag coefficient vs. TSR can be seen.

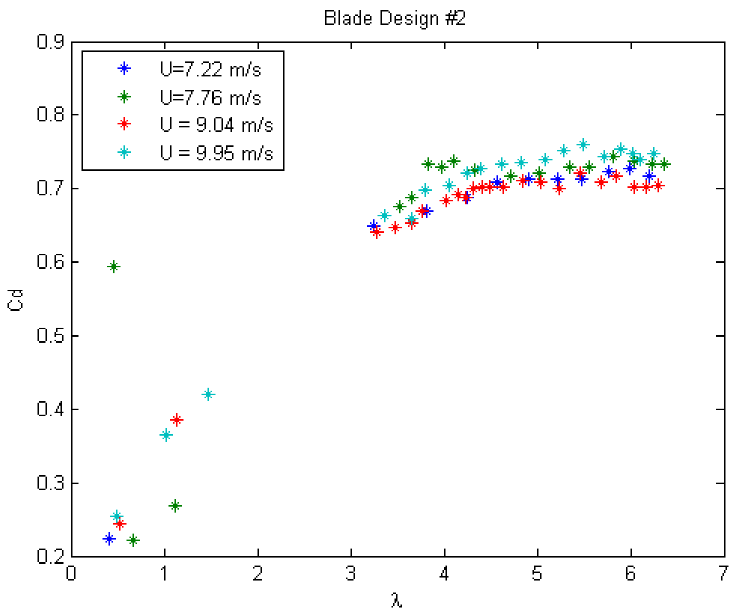

Figure 11: Coefficient of drag measurements for blade design 2

In Figure 11, it can be observed that compared to blade design 1, blade design 2 has a much higher thrust coefficient. The power coefficient data observed for blade design 2 can be seen below in Figure 12.

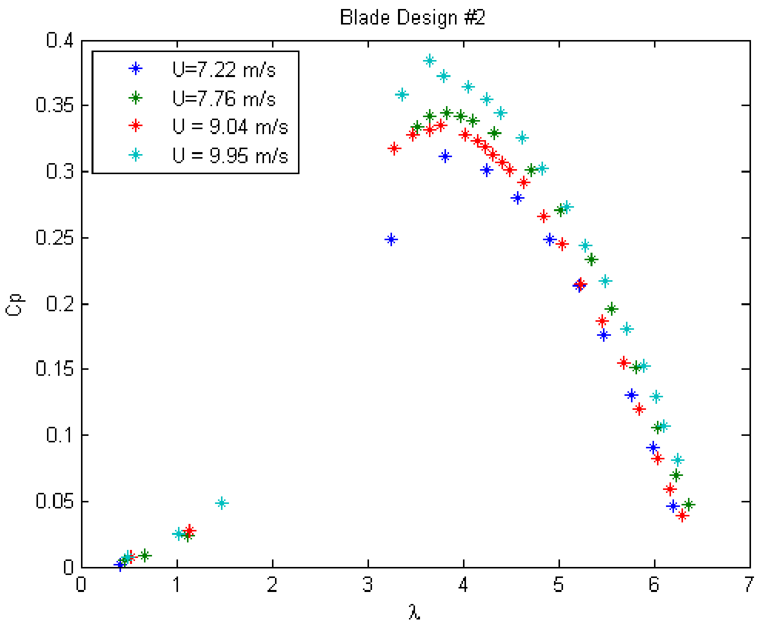

Figure 12: Coefficient of power vs. TSR for blade design 2

It can be observed in Figure 12, that the motor is not limiting the maximum output of the blade design. The design 2 can be seen to reach a maximum efficiency of roughly 35% at a TSR close to 3.75. This blade design shows the motor can measure the amount of power the target blades will achieve.

Lastly a new and final design was produced using the perfected Matlab script and a target tip speed ratio of 3.5. The airfoil was kept as a NACA 2412, and the rotor diameter was kept at 0.25m. The twist angle composed of section twist and section angle of attack, and chord length outputted by Matlab can be seen in Table 7.

Table 7: Blade design 3 characteristics

r/R	**Twist Angle** (°)	**Chord Length** (m)
0	40.3	0.0732
0.14	28.8	0.0583
0.25	21.4	0.0475
0.36	16.4	0.0396
0.46	12.8	0.0338
0.57	10.2	0.0295
0.68	8.1	0.026
0.79	6.5	0.0233
0.89	5.2	0.0211
1	4.1	0.0193

Using these blade characteristics, blade design 2 was modeled within SolidWorks and printed in ABS plastic. The entire blade and hub assembly can be seen in Figure 16.

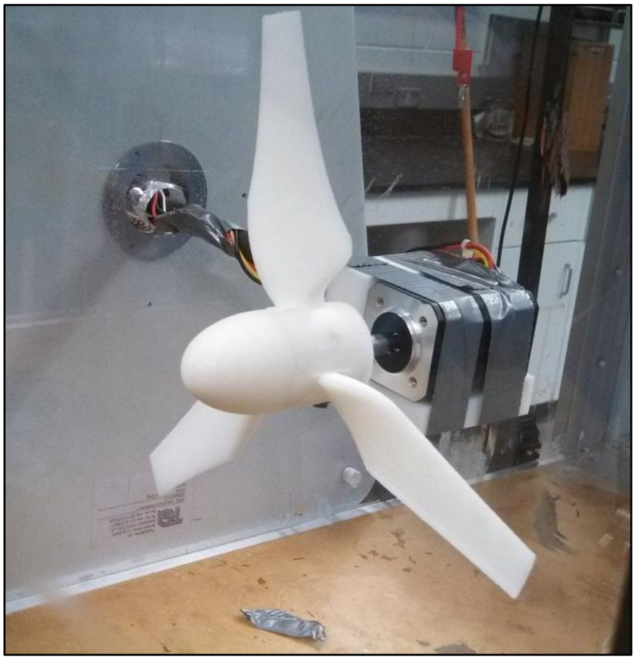

Figure 13: Blade design 3 and hub assembly

The blade design 3 and hub assembly seen in Figure 13 can be seen mounted to the 24V Anaheim Automation motor previously shown to be able to output the max power the model blades can extract from the wind. Blade design 3 was then run through the same characterization procedure as before by varying wind speed in the tunnel, and resistance on the motor, while measuring the motor current output, force balance output, and pitot tube heights. Below in Figure 14 is the drag coefficient data measured for blade design 3.

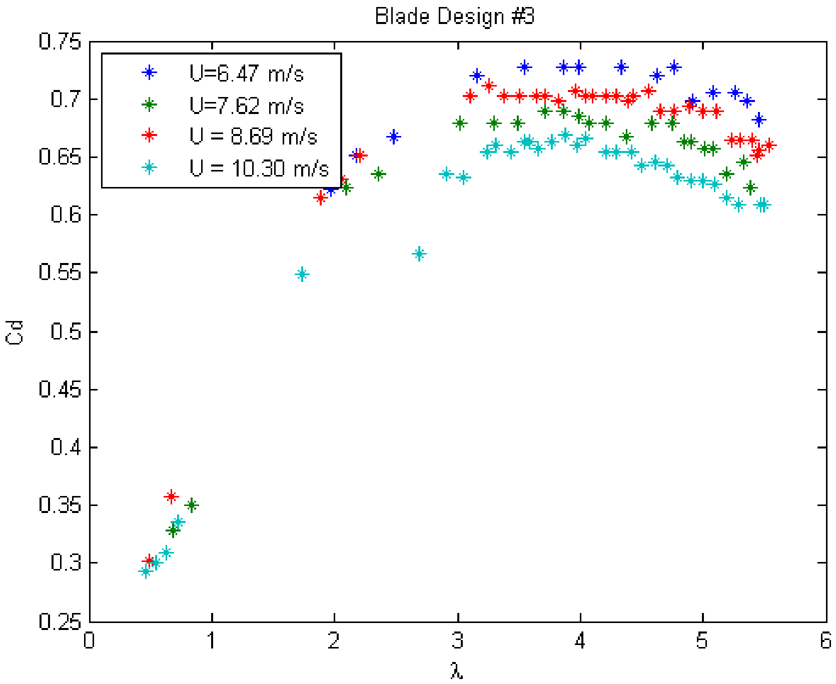

Figure 14: Drag coefficient vs. TSR for blade design 3

In Figure 20, a maximum drag coefficient is reached at the blades designed TSR of 3.5. The drag coefficient reached is roughly 0.7. The power coefficient data obtained from blade design 3 can be seen in Figure 15.

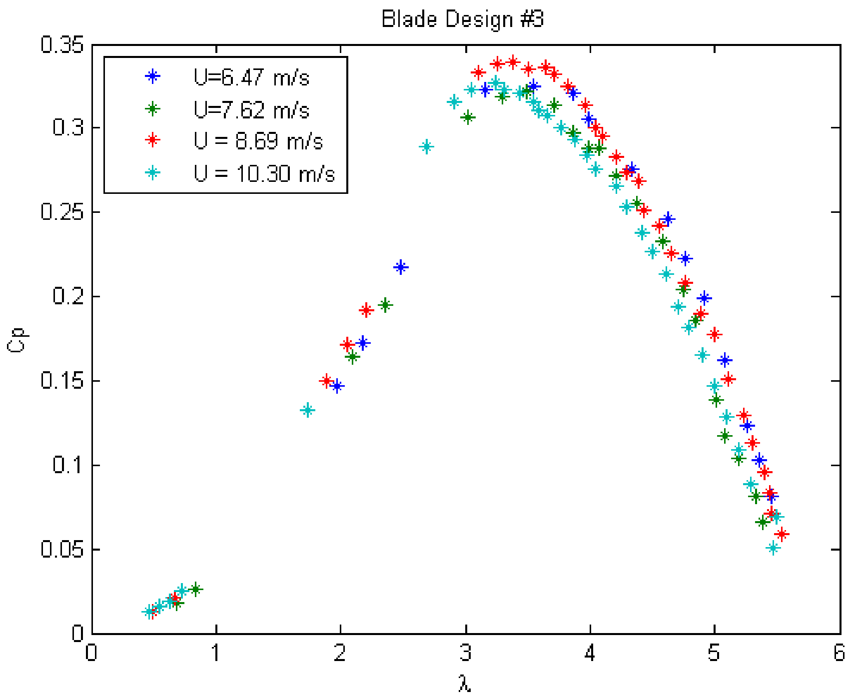

Figure 15: Coefficient of power vs. TSR for blade design 3 using 24V Anaheim Automation motor

It can be seen from Figure 15, that the Anaheim Automation motor was able to completely capture the maximum power output of the blade design. It can also be seen that a peak efficiency of 34% occurs at roughly a TSR of 3.5, exactly the TSR that the blades were designed for. This proved the BEM theory was properly used to design the model wind turbine blades.

Model Turbine Manufacturing

To quickly test the blades designed using BEM theory, the rapid prototype printer available in Kingsbury Hall at UNH proved itself to be an adequate way to quickly manufacture blades. The rapid prototype machine has a “printing” tolerance of .002 inches, which was sufficient as long as blades were oriented in a way that avoided large printing steps near thin edges, such as the trailing edge. A disadvantage of this process was the cost of material. To attempt to save money, different manufacturing methods were investigated and one alternative that was further explored was molding and casting. This was due the relatively inexpensive material costs, ability to make multiple parts at a time, and the high tolerances that could be achieved.

Casting and Molding

The initial plan to create nine turbines consisting of nine nose cones, nine hubs, and twenty-seven blades, was to create molds of the three parts and cast. The materials were purchased from a company called Smooth-On. The selected silicone used to create the molds was Mold Star® 15. Mold Star® 15 is a two part mix with a mix ratio of one-to-one volume. The pot life and cure time of Mold Star® 15 are fifty minutes and four hours respectively.

A box constructed of four pieces of plexiglass and two clamps was used to create and hold the mold as it settles. Once the mold box has been constructed a generous layer of clay must be placed inside the box on the bottom that must cover the entire floor of the box. Now the object being molded must be submerged into the clay as seen in Figure 16.

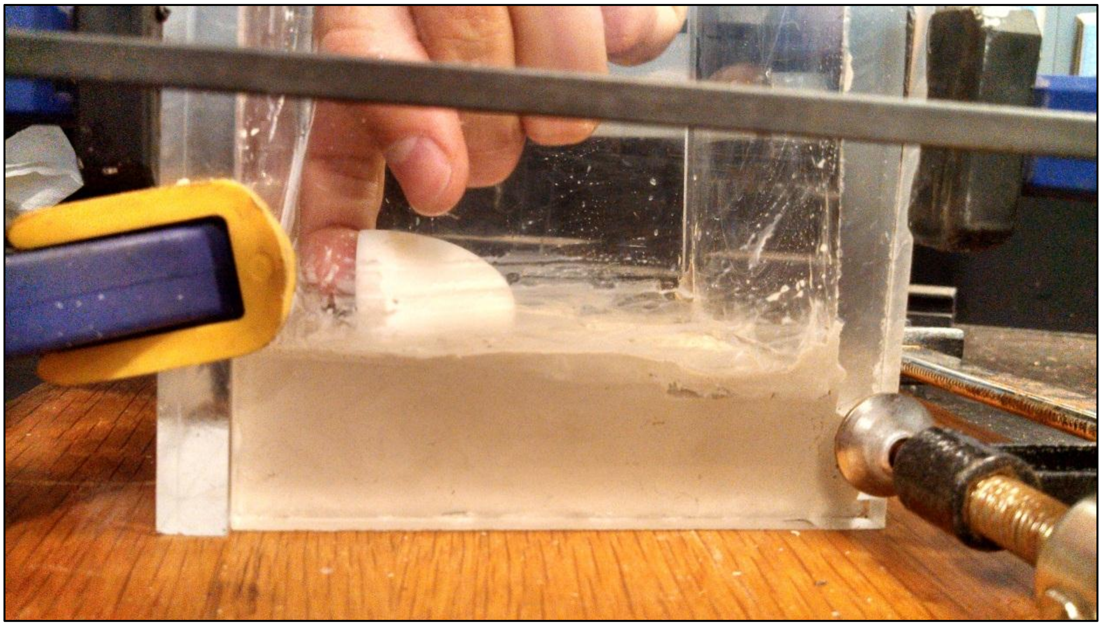

Figure 16: Mold box containing clay and object.

It was found that it was best to submerge the object up to a ridge on itself to avoid unwanted ridge lines on the casted model. With the object now in the clay, the surface of the clay must now be leveled and smoothed out in order to create keys between to the two halves of the mold for a better hold when the two halves come together. Marbles were submerged halfway into the clay to create the keys. Next equal amounts were mixed together of the two part mix and pour on top of the clay and object until the silicone mixture was about half an inch above the object as seen in Figure 17. Now the first half of the mold was allowed to cure.

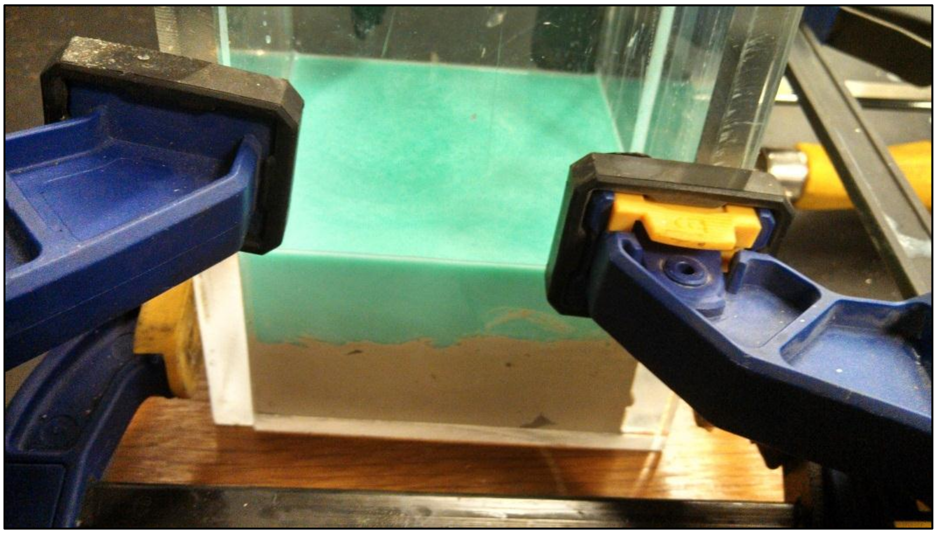

Figure 17: First half of the mold curing.

Once the mold had cured the sides of the box were taken off and the clay and marbles were removed while keeping the object in the mold. With the silicone clean, the box was replaced around the mold and refastened. Before mixing more silicone to make the second half of the mold, the object and first half of the mold in the plexiglass box was sprayed thoroughly with Ease Release® 200 to avoid the silicone halves sticking to each other. The second half of the silicone mixture was then poured into the box and allowed to cure. Once the second half was allowed to cure the mold was taken out of the box and the object out of the mold. A keyhole must was cut into the mold where the plastic resin will be poured through as seen in Figure 18.

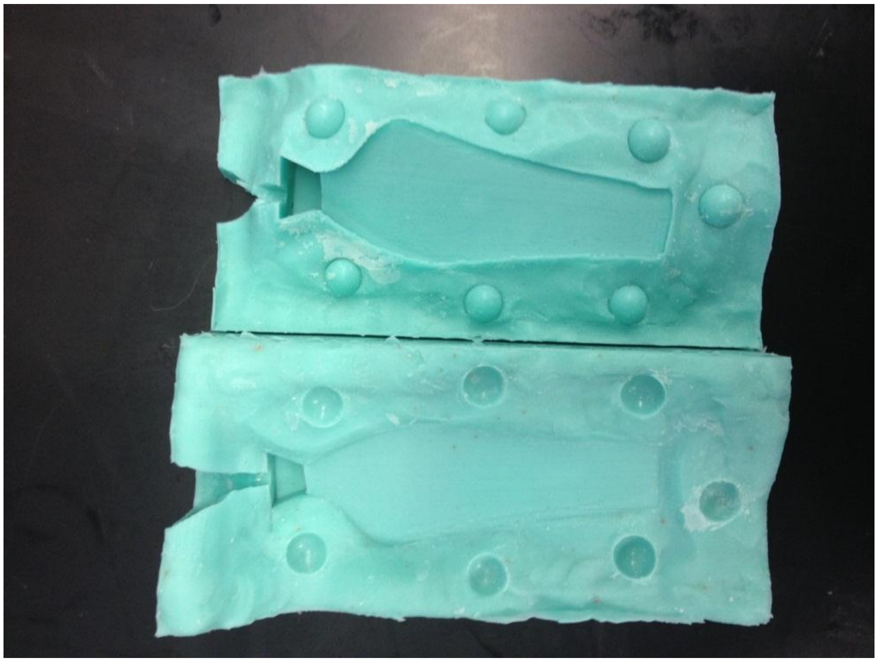

Figure 18: Complete mold of turbine blade for design 3

The plastic resin chosen for our casting was a urethane plastic called TASK®3 because it offered a high tensile strength and was used for making prototype models. The mix ratio for TASK®3 was also one-to-one with a pot life and cure time of twenty minutes and ninety minutes respectfully. After the plastic resin has been mixed, poured, and cured the model was removed from the mold and sanded down as necessary.

Rapid Prototyping

Rapid prototyping is a process commonly used in three dimensional modeling. The first step to create the model is making a 3D drawing in an engineering diagramming package such as SolidWorks. This part is then uploaded to the rapid prototyping machine which breaks down the part into many tiny discrete part. The printer then prints out the bottom layer first followed by the remaining sections one by one in ABS plastic. This technique is a quick and easy way to create a 3D model.

There are several factors that were extremely important in the manufacturing process of the turbine blades. The first factor was the strength of the blades. Because the rapid prototype machine used the same process to create the parts the stiffness of the parts were extremely consistent. Another important factor in manufacturing the turbine blades was the surface finish of each blade. To keep each turbine as consistent as surface finishes between blades had to be very similar. The tolerance of the rapid prototyper was also important. With a minimum tolerance of .002 inches, it was important that nothing in the blades design was smaller than that or it would not be printed properly. The casting and molding could cause a rough surface finish for the blades caused from air pockets and bubbles. One problem did exist with the rapid proto typing machine. While printing the blades in the rapid prototyping machine the wings must be orientated with the trailing edge pointed straight up or the blades would be printed with inconsistencies. Another problem was the cost of the rapid prototyping. The cost to use this machine along with the material was $\$10/in^3$. For the fabrication of all parts for nine model turbines, the rapid prototyping process was more than twice as expensive as the casting.

Tower and Hub Manufacturing

The hub height of the turbines is defined as the distance from the ground to the middle of the diameter of the blades. The hub height of the turbines is to be three quarters of the blade diameter. With a blade diameter of 25cm the hub height was determined to be 18.75cm. Subtracting half of the motor height and thickness of the L-bracket used to mount the motor from the theoretical hub height resulted in a value of 16.3cm. Thus eight rods were cut to the length of 16.3cm. The rod is made of 1566 steel with a diameter of 3/8". The bottom of the rod must be threaded into a baseplate which will prevent the baseplate from tipping over or slipping. The bottom of the rod must be threaded to a length of 2.5cm. The top of the rod will be screwed into an L-bracket that is 3/16" thick. Thus the top of the rod will have a thread of length 1.3cm. Before the baseplates or L-brackets are screwed onto the rod a square nut with a height of ¼" must be screwed on first. The presence of the two nuts will allow the turbine to be arranged in any direction possible while also maintaining the ability to tighten the turbine preventing it from turning.

The threaded rod is screwed into a baseplate that is comprised of 1018 carbon steel. The baseplate is ½" thick preventing the baseplate from effecting the flow and boundary layer. The length and width of the baseplate are 6"x6". The 6"x6" dimensions were chosen to prevent the turbines from sliding or tipping over. An analysis was performed by calculating moments caused by the force of the wind acting on the turbines and the weight of the turbine including the weight of the baseplate. The analysis determined that the baseplate must have a volume of approximately 10in^3. As a precaution a volume of 18in^3 was selected. The baseplate was then drilled with a 3/8" hole in the center which was then threaded to match the threaded rods.

The L-brackets that thread to the top of the threaded rods have a thickness of 3/16". The leg of the L-bracket that screws onto the threaded rod were also drilled and threaded to match the same parameters of the baseplates. The leg that screws onto the threaded rod has a length of 1 ½". The front leg that is mounted to the motor was milled down from the top to properly mount the motor flush. Two holes were also drilled in the front leg of the brackets where screws were then used to mount the L-bracket to the motor. After the motor has been set in place on the L-bracket the hub of the turbine can be press fitted onto the motor shaft. To finish the construction process the turbine blades and nose cone can be assembled.

Construction of force balance

To characterize the blades of each turbine in a given array formation the drag force on each turbine in the array had to be quantified. One of the turbines was placed on a linear slider aligned with the direction of the velocity field in the Flow Physics Facility (FPF) at the University of New Hampshire. The flow caused a drag force on the turbine that directly applied a force to a 5lbf high sensitivity load cell. This load cell was chosen due to the low magnitude of forces that were expected to be experienced by the turbine attached to the force balance. The load cell outputted a voltage reading into a data file that corresponded to a specific force. The turbine was then placed in various locations downstream from the additional turbines in order to find an efficient spacing for the study.

The 5lbf load cell was purchased and statically mounted onto a table. An excitation voltage of 10V was applied to the load cell and the output voltage was used to calibrate the load cell. Calibrated weights were then hung from the load point.

Figure 19: 5lbf load cell used in the force balance assembly.

This data was then used to construct a calibration curve to find corresponding output voltages for various different weights. Error had to be calculated for this design to account for the minimal friction in the system as well as the load cell not being directly attached to a force point caused from the flow field on the turbine blades. A string that was considered to be massless was connected to the rear end of the turbine. The string was applying a force directly in the center of the turbine. The opposite end of the string was attached to a pulley that can be assumed to have zero friction. Various different calibrated weights were hung from the string and the output voltages of the load cell were recorded, this produced a calibration curve for the system.

The force balance assembly was first constructed with a 6” x 6” x 3/8” piece of unpolished (cold Drawn) 1018 carbon steel which acted as the baseplate. This piece had two 3.6” linear ball bearing sliders statically mounted parallel two each other on the baseplate. An aluminum plate was then mounted to the top of the sliders allowing this plate to slide with minimal friction. A 3/8” hole was tapped and threaded through the center of the aluminum plate. A 3/16” L-bracket was then threaded to the original baseplate to statically mount the 5lbf high sensitivity load cell resting against the linearly sliding plate. A 3/8” diameter 5.512” in length 1566 steel rod was then threaded on the last inch of each end and mounted onto the aluminum sliding plate in the previously threaded hole. A 3/16” L-bracket was then threaded to the opposite end of the shaft that housed a 24V DC electric motor that acted as the generator for the 9.84” diameter turbine.

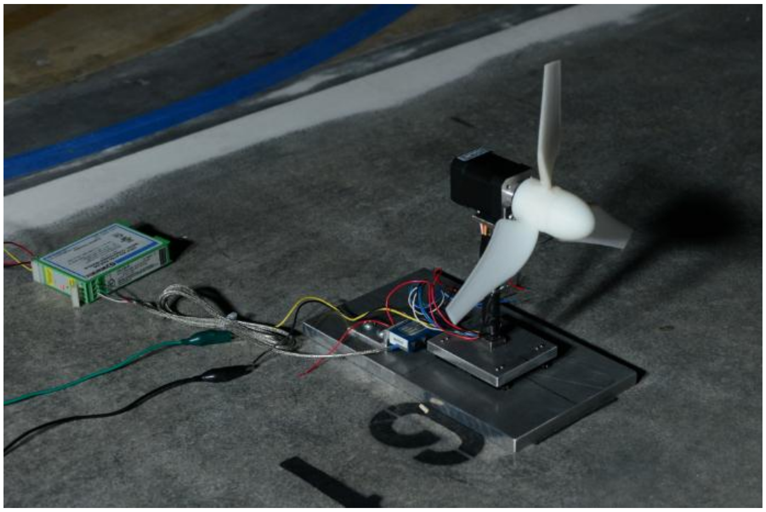

Figure 20: Force balance setup for model turbine in UNH Flow Physics Facility.

When the force balance was completed, the entire force balance was calibrating using calibration weights and a rig which applied a force in a similar fashion that the turbine would be experiencing during testing. The calibration curve can be seen below in Figure 21: Calibration curve for turbine force balance.

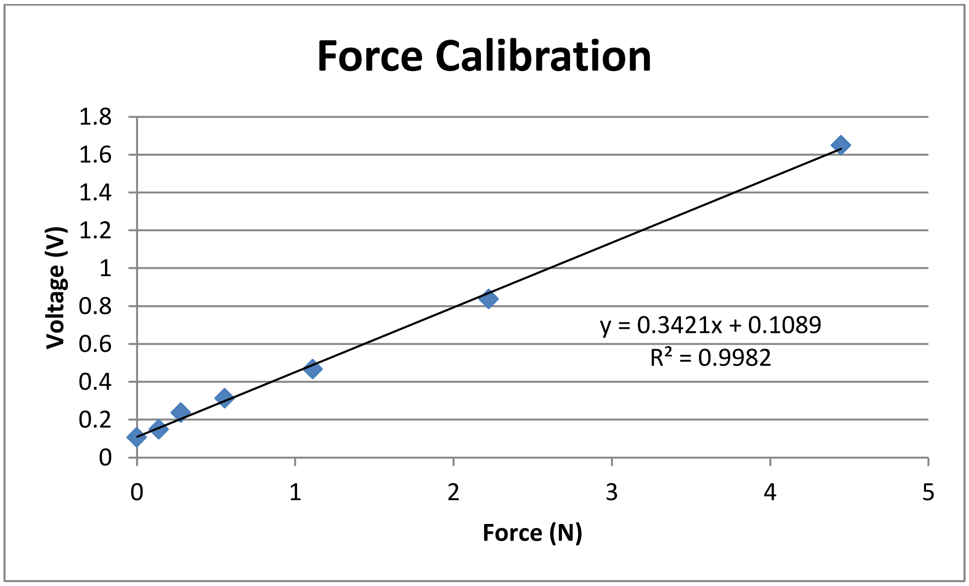

Figure 21: Calibration curve for turbine force balance

Flow Physics Facility Experimentation

Turbine Blade Characterization

The turbines were moved to the FPF wind tunnel in order to validate the findings from the student wind tunnel by again characterizing the blades within the free stream velocity and then moving the same turbine back into the turbulent boundary layer of the FPF to investigate how the turbine will perform compared to free stream. The characterizations of the turbines were performed using the same method as used in the student wind tunnel where a potentiometer was used to vary the load on the model turbine. The National Instruments NI-PXI-1042 data acquisition was used to record continuous data for one minute at 2000 Hz. After one minute the potentiometer's resistance was manually decreased, starting at 100Ω and incrementally decreasing to 0Ω.

Theory

To compare the data collected in the student tunnel to the data collected in the FPF the velocity field and wind speed had to be consistent for both cases. In the student wind tunnel the testing section was in free stream velocity. To accurately model this velocity field in the FPF the testing section had to be above the boundary layer at the front of the wind tunnel where the boundary layer is initially tripped and is the smallest. Figure 22 shows a schematic of the turbine being tested in the free stream velocity field.

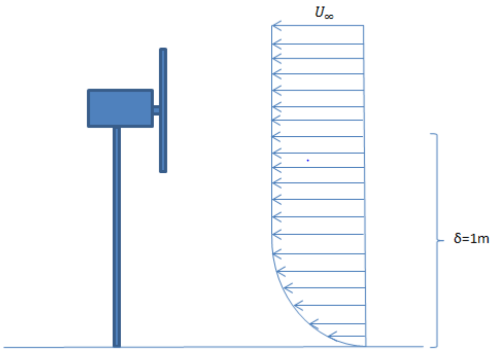

Figure 22: Schematic illustrating testing of wind turbine in the free stream in the UNH Flow Physics Facility.

Once the testing in the free stream was complete the testing section was moved to the back of the wind tunnel in the turbulent boundary which is comparable to the atmospheric boundary layer where the actual turbines would be operating. As shown in Figure 23 the velocity field will be fully developed when it interacts with the leading turbine. Directly behind the leading turbine there will be a deficit in this flow produced by the wake caused by the leading turbine **[10]**.

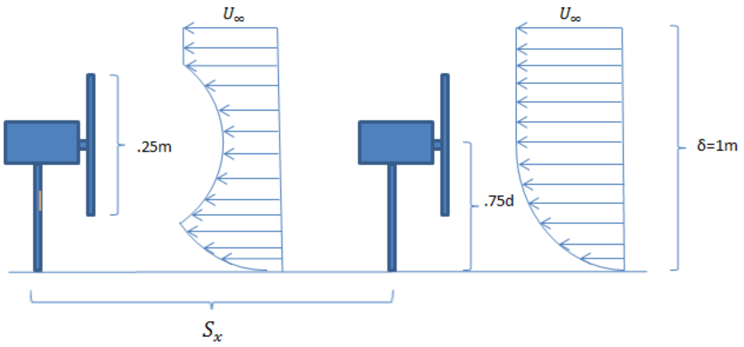

Figure 23: Schematic illustrating testing of wind turbine in the boundary layer (right turbine) and the velocity deficit experienced by the downwind turbine (left turbine).

This trailing velocity field has a deficit when it interacts with the trailing turbine. This will cause the trailing turbine to have a lower power output. As velocity readings downstream are measured it can be noted that if the flow is not disturbed the deficit will slowly decrease until the flow is finally fully developed and the trailing turbine will output the same amount of power as the leading. With that being said, as the spacing is increased the power output of the trailing turbine will increase creating a more efficient array. Figure 24 is an actual picture of an offshore wind farm, Horns Rev1. It shows the effects of leading turbines on the trailing ones behind it.

Figure 24: Photograph of Horns Rev 1 that depicts effects of leading turbines on trailing

Meteorological conditions at Horns Rev I made the wake effects from upstream wind turbines visually apparent through cloud formation that occurred on 12 February 2008. Photo courtesy of Vattenfall **[13]**

Free Stream

The free stream performance curve can be seen below in Figure 25. It should be noted that each data point on the graph is the average value from one minute of continuous data recorded at 2000 Hz.

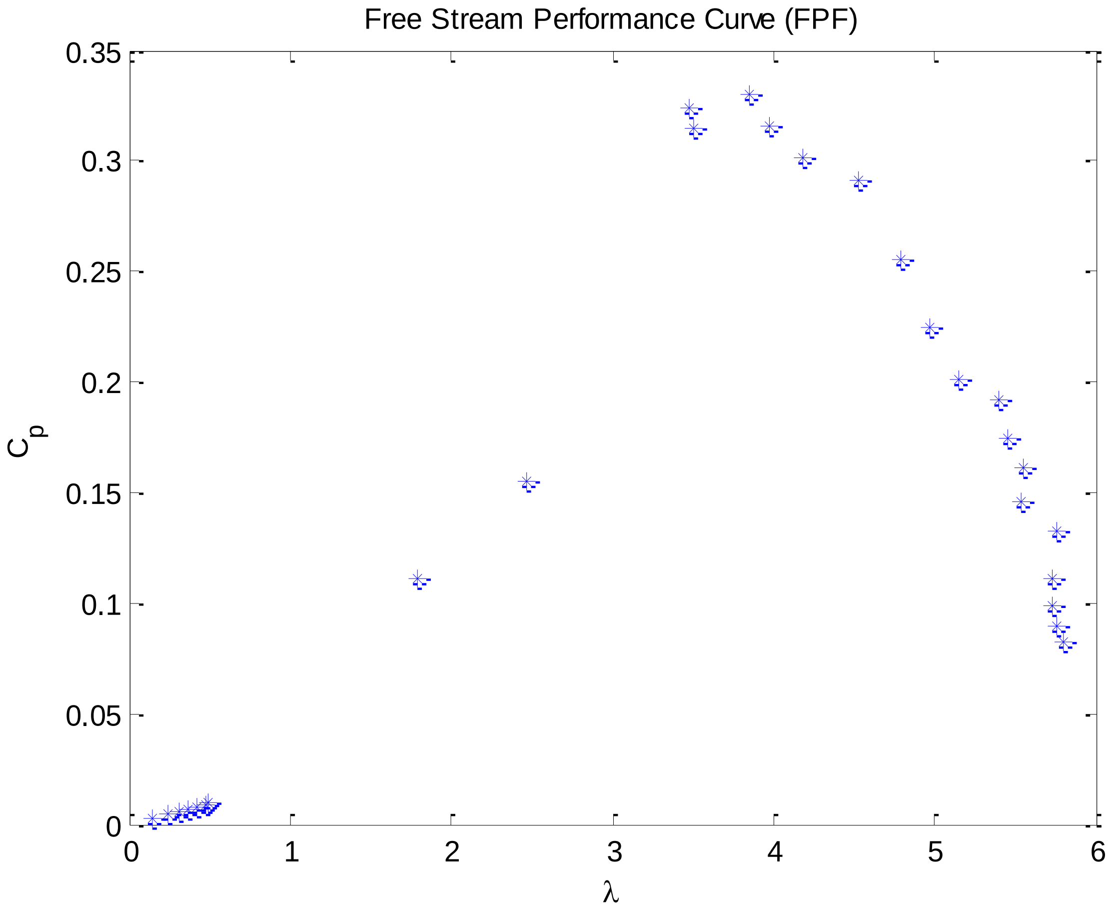

Figure 25: Performance curve of blade design #3 in free stream of FPF

From the above figure, it can be seen that the maximum power coefficient peaks at slightly below .35. This peak efficiency occurs at a tip speed ratio of 3.5, the exact TSR that the blades where designed to run at using 1-D BEM theory. It should also be noted that when comparing to the free stream testing performed in the student wind tunnel, Figure 15 the results are very close to what was found in the FPF. The blades perform nearly identically in both wind tunnels. With the peak C_p reaching slightly below 35%, and that peak occurring at a TSR of 3.5.

Turbulent Boundary Layer

With the blade design validated in the free stream of the FPF, the model turbine and data acquisition system where moved back 61m into the turbulent boundary layer portion of the tunnel, to see how well the blades would perform compared to how they did in the free stream. Below in Figure 26 is the performance curve of the blades that was taken in the turbulent boundary layer.

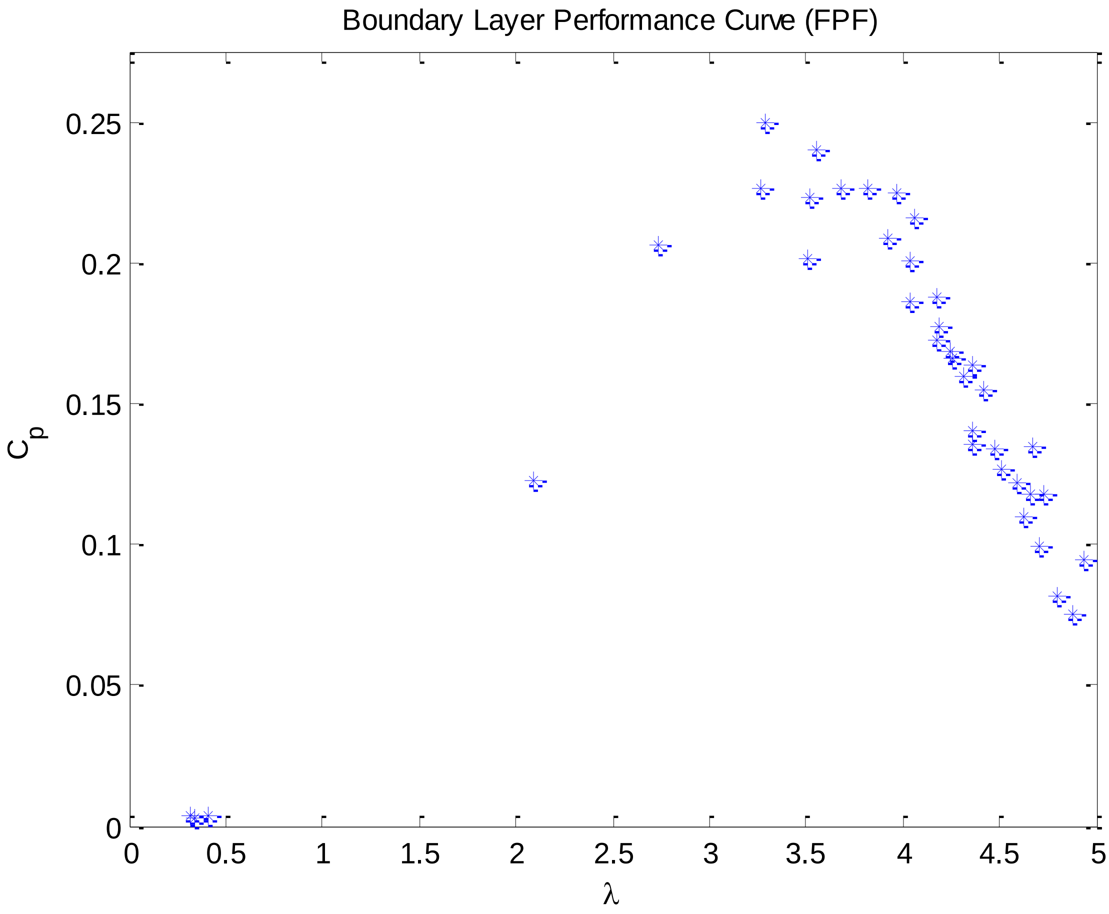

Figure 26: Performance curve of the blade design three in the turbulent boundary layer of the FPF

The above plot shows how the turbine behaves differently in the boundary layer than it does in the free stream. Most notably, it can be seen that that turbine runs at a C_p that is roughly 10% less than that in the free stream. This is to be expected though, just as the name states, the turbulent boundary layer is a turbulent area to operate in. The velocity field is erratic, and inconstant and measurably slower than the free stream. It is not the same clean consistent flow that is seen in the free stream. It is this variable flow that causes the turbine to not run as efficiently. It should be noted though, that once again the maximum efficiency peaks around the TSR of 3.5.

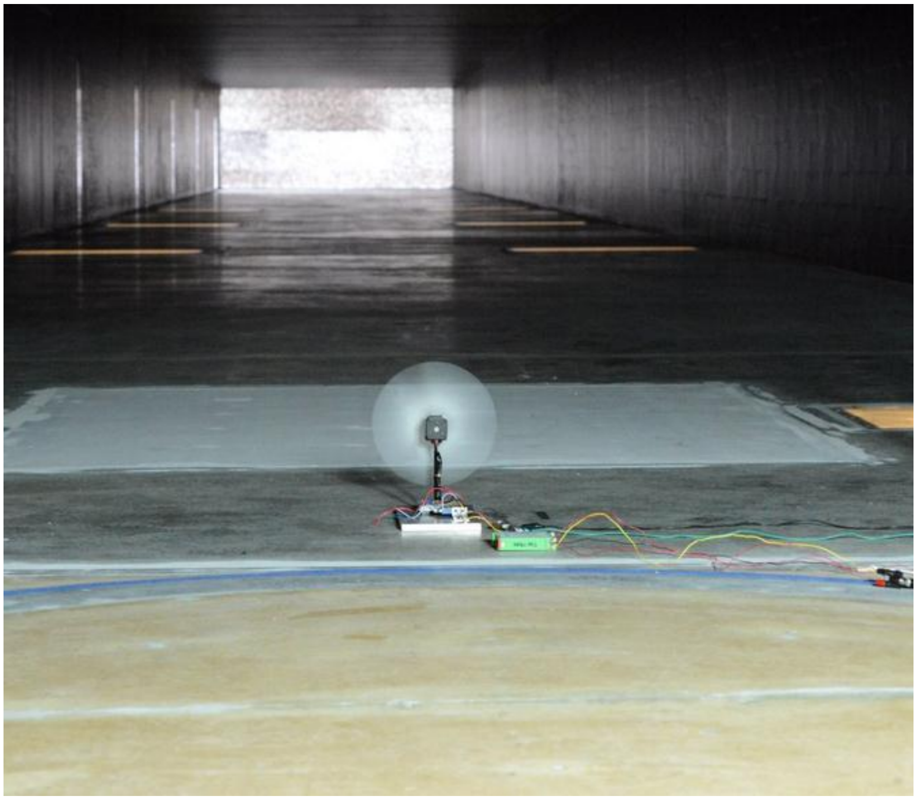

Figure 27: Model turbine attached to force balance in turbulent boundary layer of FPF

Array Spacing Studies in Turbulent Boundary Layer

After completion of the blade characterization in the free stream and turbulent layer of the FPF array configurations were investigated. To begin, Figure 26 was used to determine what load to apply to each of the motors in the array. A resistance of 47Ω was chosen to load the motors. This resistance corresponds to the turbine running at a TSR of roughly 4.25. Although the motor was designed to run most efficiently a TSR of 3.5, the turbines were chosen to run higher due to the fact that at a lower TSR the stall torque on the motor was high enough where the trailing turbines would not start spinning when spaced too closely together.

The first array analyzed was a continuation of the turbine analyzed in the turbulent boundary layer. This was done by placing a turbine six diameters in front of the force balance turbine to create a 2x1 array. The wind tunnel was operating at 6.67 m/s and data was collected using the NI-PXI-1042 data acquisition system for a total of 5 minutes at $2000Hz$ and then averaged. The data collected was the voltage from the motor output, the output of the wind velocity from the pitot tube set up given in Torr, and the voltage output of the load cell attached to the custom made force balance. At the completion of five minutes, the spacing between the two turbines was increased by one diameter so a total of seven diameters was between the turbines. Again, data was collected for another five minutes and averaged. This process was repeated until the spacing between the two turbines was twelve diameters. After the twelve diameter spacing test was complete a third turbine was added in line with the other two turbines creating a 3x1 array. The spacing between the three turbines was reset at six diameters. Once again data was collected at five minute intervals for spacing of six diameters up to twelve diameters. The process of adding turbines increased until there were six turbines in a 6x1 formation. The results from the 6x1 array can be seen in Figure 29

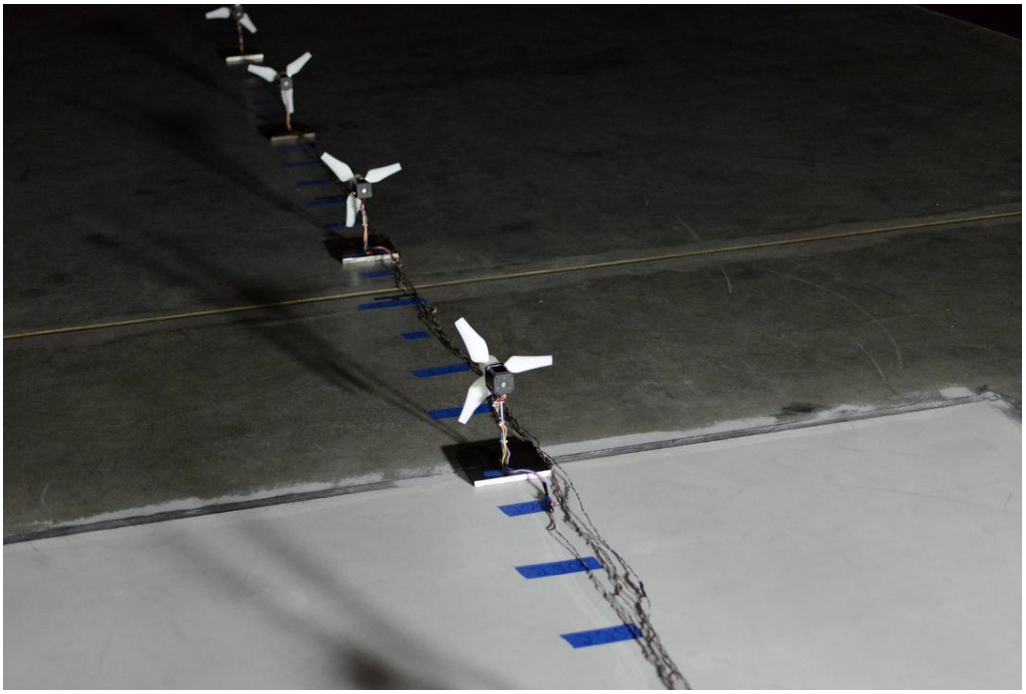

Figure 28: Experimental setup of 6x1 array in turbulent boundary layer of FPF

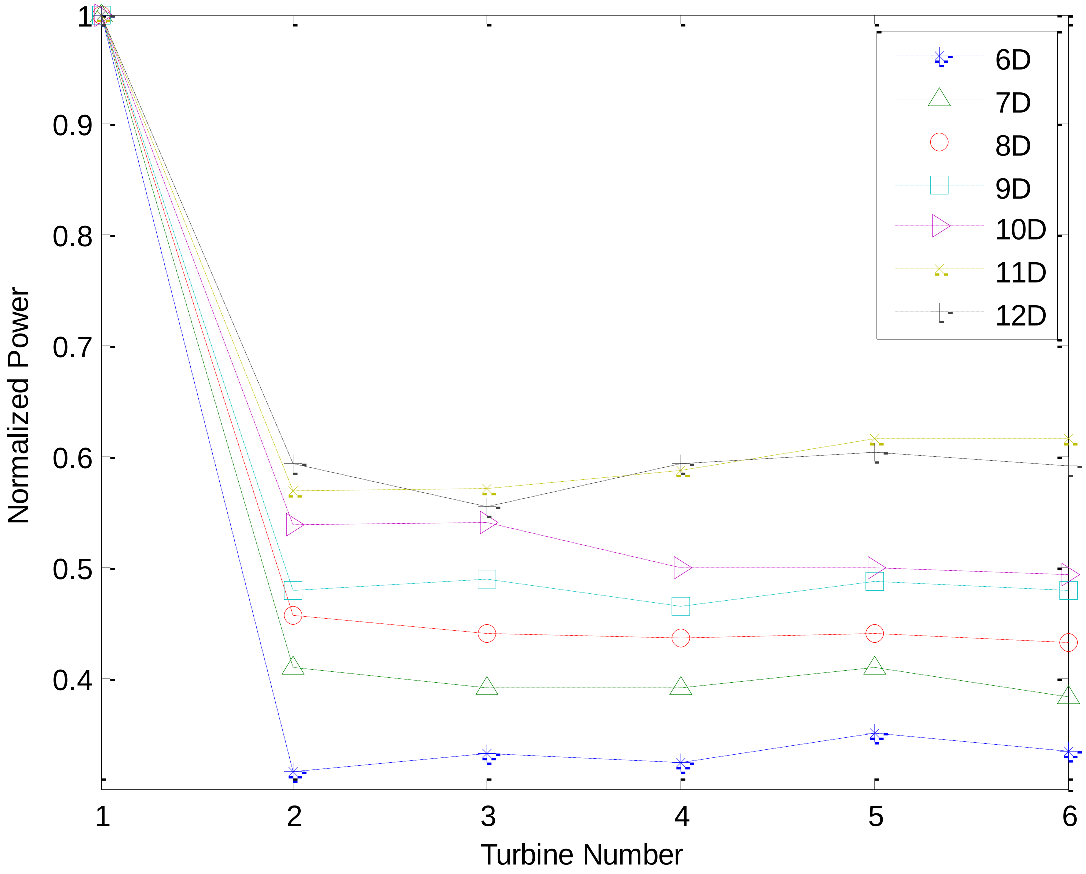

Figure 29: Normalized power vs. turbine number at various spacing in the FPF

The above figure is normalized power versus turbine number. Where normalized power is simply the ratio of power the trailing turbines are extracting compared to the leading turbine in the array. Some trends can be seen from the above data. For a 6x1 array of the model turbines spaced 6 diameters apart, the trailing turbines behind the first in the array are all individually extracting less than 35% of the power than the leading turbine. When spacing between turbines was increased incrementally in 1 diameter spacing the power output of the trailing turbines increased as expected. By the maximum spacing between the turbines, 12 diameters apart, the individual power extraction of the trailing turbines has increased to 60% of the leading turbine. One interesting trend that can be seen from Figure 29 is how each trailing turbine after the first all are extracting nearly the same amount of power even when the turbine is placed at positions in the array. This phenomenon is due to the fact that the first turbine is not only creating a velocity deficit behind itself, it is also creating a momentum deficit. To make for this momentum deficit, there is a momentum flux that is feeding the trailing turbines that is coming from the sides and above the turbines. It is the equal spacing of the turbines that is causing all the trailing turbines to have nearly the same power output.

During the 6x1 array testing thrust data was also being collected from the trailing turbine. The data can be seen below in Figure 30.

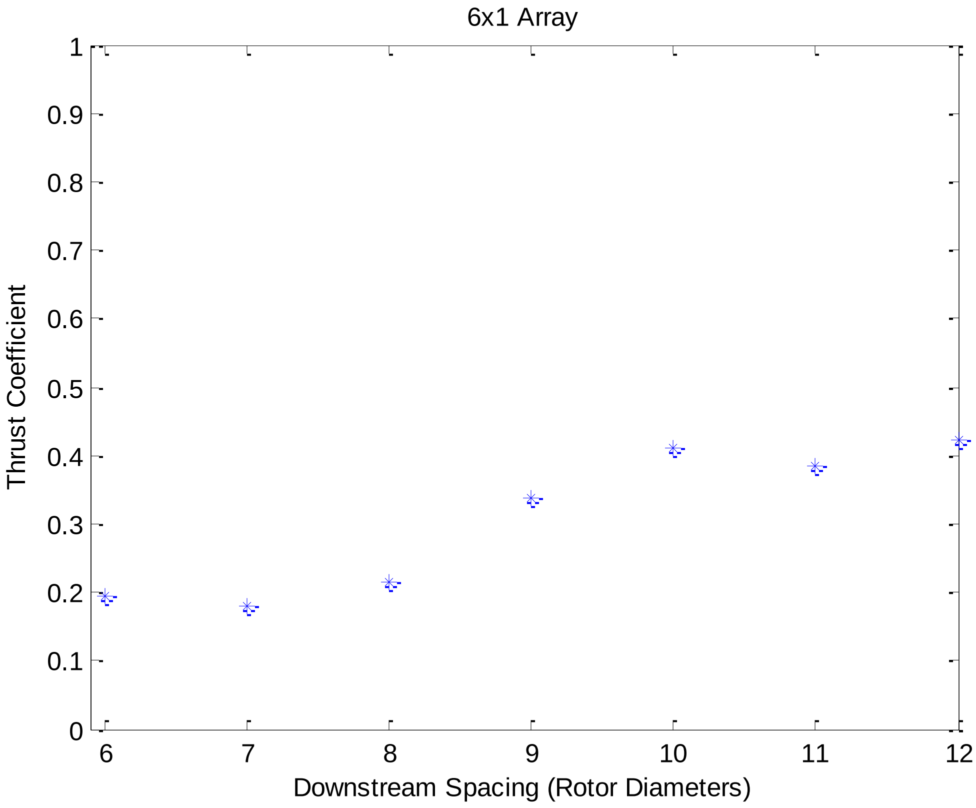

Figure 30: Thrust coefficient for last turbine as spacing between all turbines was increased

In the above figure, of thrust data versus turbine spacing, the trend can be seen as spacing between the turbines was increased; the thrust force acting on the turbine was also increasing. At 6 diameter spacing, the thrust coefficient of the trailing turbine was slightly below 0.2, as spacing was increased to 12 diameters, the thrust force acting on the trailing turbine was now at slightly above 0.4. This trend is to be expected. From Figure 29, it was seen that even at 12 diameter spacing between turbines, the trailing turbines were still extracting significantly less power than the leading. If the spacing was increased greatly to where the trailing turbine was extracting the same power as the leading, it would be expected that the turbine would have a C_t of around 0.7, the designed thrust coefficient that was observed in the student wind tunnel.

After the 6x1 array was studied, an investigation was done to find how many diameters was required between turbines for the velocity field behind the first to fully recover so the trailing turbine had equal power extraction to the leading. A plot of normalized power vs. array spacing can be seen below in Figure 31.

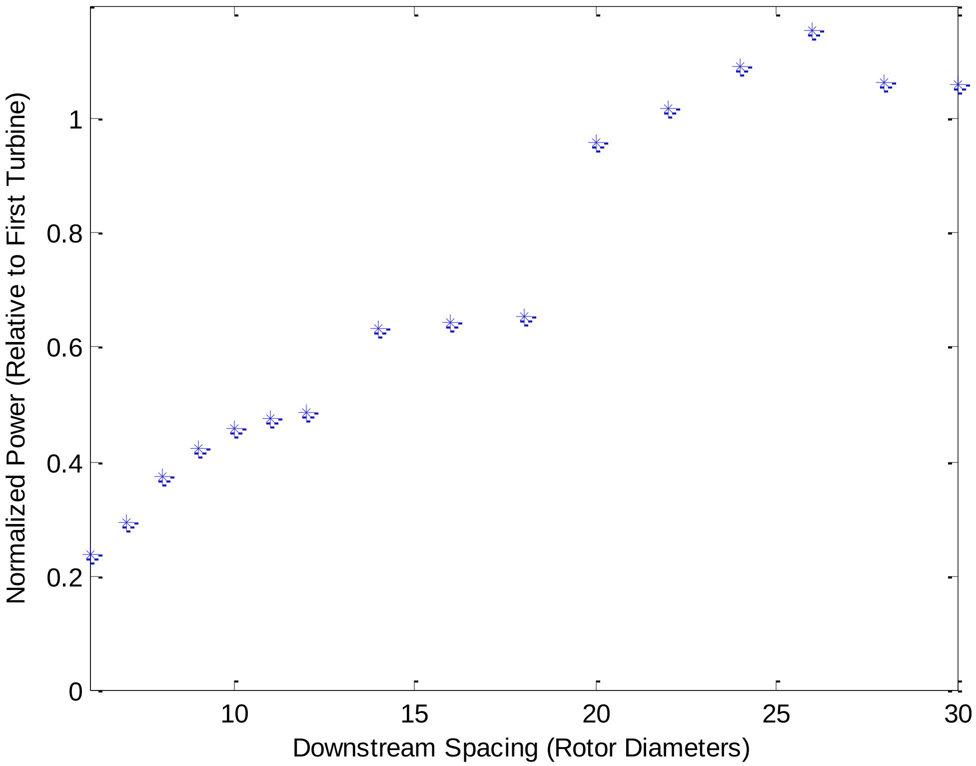

Figure 31: 2x1 array where spacing was increased until trailing turbine extracted the same power as the leading turbine.

In the above plot of normalized power vs. increasing diameter spacing between the two turbines it can be seen how increasing spacing between turbines increases power output of the trailing. Most notably, it can be seen that it takes right around 20 diameters between turbines for the velocity field to recover enough for the trailing turbine to be able to extract the same amount of power as the first. It should be noted that this was simply a 2x1 array. For any larger arrays, it is unknown if 20 diameter spacing between turbines would be adequate.

Summary and Conclusions

This project investigated how wind turbine spacing affects turbine and array power output, using small arrays of scaled model wind turbines. A total of nine realistically scaled models of 5MW offshore wind turbines were designed, fabricated and characterized with respect to performance. Wind turbine arrays of various configurations (e.g., arrays of 1xN, 1x9, 3x3 turbines) were installed and tested in a high Reynolds number turbulent boundary layer in the UNH Flow Physics Facility. Turbine spacing was varied, power output, tip speed ratio and thrust of turbines were measured, and array power was correlated to array area.

This study proved wind turbines operate at higher power coefficients in a uniform velocity field (free stream) than in a boundary layer due to the unsteady turbulent shear flow in the boundary layer. The first turbine in an array was found to extract the most power from the wind, causing a velocity deficit behind it that affects power extraction for the trailing turbines. Power extraction for trailing turbines can be increased with increased spacing. It was demonstrated with a 2x1 array study that it takes approximately a spacing of 20 turbine diameters between turbines for the velocity field behind the leading turbine to recover sufficiently, so that the trailing turbine can extract the same amount of power as the leading turbine. The data obtained with this study can inform cost-benefit analyses on the layout of very large wind farms. Increasing spacing will result in more power extraction, however, the cost of ocean area used, power cables, labor, materials will also increase.

Additional studies to investigate how different array configurations affect power output are possible with the experimental setup. One configuration in particular that will be studied will be two-dimensional arrays, where spanwise and streamwise spacing will be systematically varied, and power extraction of the turbines in the array compared.

Bibliography

[1] Schreck, S., Lundquist, J. and Shaw, W., "U. S. Department of Energy Workshop Report: Research needs for wind resource characterization", National Renewable Energy Laboratory Technical Report, NREL/TP-500-43521, 2008.

[2] Schlez W; Neubert A; Smith G (2006) New developments in precision wind farm modeling, GermanWind Energy Conference DEWEK 2006, Bremen, Germany.

[3] Sheinman Y, Rosen A (1992) A dynamic model of the influence of turbulence on the power output of a wind turbine. J Wind Eng Ind Aerodyn 39:329–341.

[4] Medici D, Alfredsson P (2006) Measurement on a wind turbine wake: 3D effects and bluff body vortex shedding. Wind Energy 9:219–236.

[5] Medici, D. and Alfredsson, P. H. (2005). Wind turbine near wakes and comparisons to the wake behind a disc. ASME Conference, January 2005, Reno, Nevada. AIAA-2005-0595

[6] Medici, Davide. "Experimental Studies of Wind Turbine Wakes - Power Optimisation and Meandering." Thesis. Royal Institute of Technology, 2005. Web. 11 Feb. 2013.

[7] Fox, Robert W., Philip J. Pritchard, and Alan T. McDonald. "External Incompressible Viscous Flow." *Fox and McDonald's Introduction to Fluid Mechanics.* 8th ed. Hoboken, NJ: John Wiley & Sons, 2011. 439-40. Print.

[8] Manwell, J., McGowan, J., andRogers, A.(2002). Wind Energy Explained.Theory, Design and Application. John Wiley and Sons, Ltd

[9] Barthelmie R., Hansen K., Frandsen S. T., Rathmann O." Modelling and Measuring Flow and Wind Turbine Wakes in Large Wind Farms Offshore "Wiley Interscience Wind Energ. 2009; 12:431–444

[10] Barthelmie, R. J. et al "Quantifying the Impact of Wind Turbine Wakes on Power Output at Offshore Wind Farms." *Journal of Atmospheric and Oceanic Technology* 27 (2010): 1302-316. Print.

[11] "Annual Energy Review 2011." *U.S. Energy Information Administration*. Department of Energy, 27 Sept. 2012. Web.

[12] "20% Wind Energy by 2030-Increasing Wind Energy's Contribution To U.S. Electricity Supply." *Department of Energy-Energy Efficiency and Renewable Energy*. N.p., July 2008. Web.

[13] Stark, Anne M. (2011) In the Wake of Wind. Lawrence Livermore National Laboratory NR-11-04-06 (26 Apr. 2011). Web.

Acknowledgments

- This work is the result of research sponsored in part by the New Hampshire Sea Grant College Program through NOAA grant # NA10OAR4170082, and the UNH Marine Program.

- This work was also sponsored by the Mechanical Engineering Department at the University of New Hampshire through the departments differential student funds.

Appendix

Porous Disk

Theory

According to Medici & Alfredsson [4], porous disks can produce down-stream flow conditions similar to wind turbines. For proper comparison, these disks must have comparable thrust (=drag) coefficients the full scale turbines. Tabulated thrust coefficient data for an Enercon 2.2MW, a Nordex 2.5 MW, and a Siemens 3.0 MW are shown below. Note that the terms drag coefficient and thrust coefficient are synonymous, the latter being used in the wind industry to express a non-dimensional axial force on the rotor.

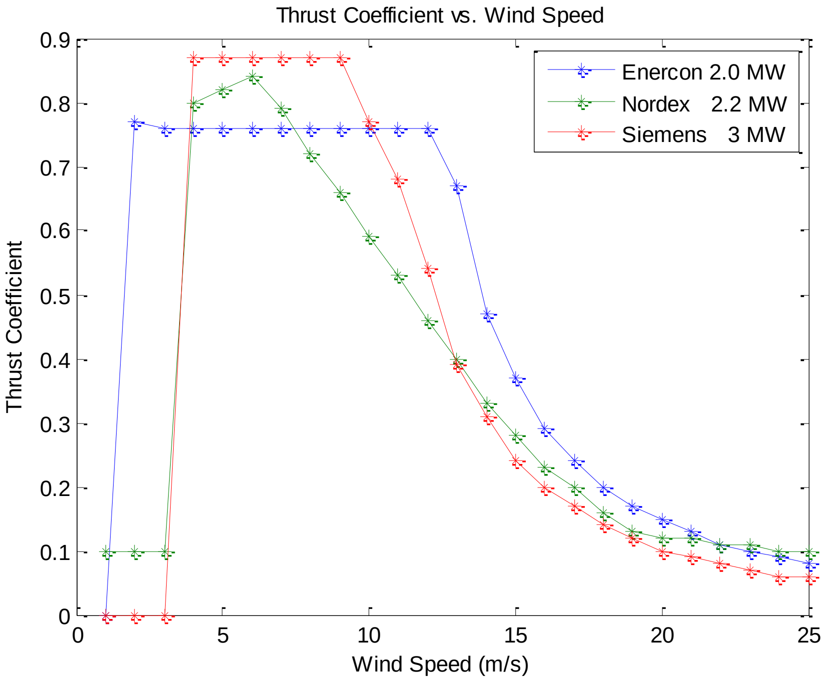

Figure 32: Thrust coefficient curves for three utility scale turbines

As mentioned previously, the wind farm experiments will be carried out with a free stream wind speed of ~7 m/s. The thrust coefficients of the utility-scale turbines shown in Figure 4 are ~0.8 at 7 m/s. From 1-dimensional momentum theory it can be shown the thrust coefficient for an ideal wind turbine rotor is $C_T = 4a(1-a)$, where a is the induction factor, defined as the fractional decrease in wind speed at the rotor plane. With a=1/3 for maximum power coefficient C_p (Betz limit), the corresponding thrust coefficient becomes 8/9, or about 0.89. To match 1-D momentum theory, the porous disks and future small scale model turbines, had a target thrust coefficient of 0.8.

Experimental Procedure

Different porosities were tried to achieve this target thrust coefficient of 0.8. Three types of porous sheets were purchased from McMaster-Carr. The specifications of the porous sheets are shown below in Table 8.

Table 8: Specifications for the porous disks used for experimentation

Porosity	0.32	0.40	0.48
Sheet Thickness	0.188 in.	0.188 in.	0.25 in.
Center-to-Center Spacing	0.313 in.	0.563 in.	0.688 in.
Hold Diameter	0.1875 in.	0.375 in.	0.5 in.

The sheets of porous material were machined into porous disks with three different diameters, 3”, 5”, and 10”. The different diameters were used to investigate the effects of blockage in the wind tunnel. The different disk diameters also allowed a wider range of Reynolds numbers to be covered.
The drag measurements for the porous disks were conducted in the small aerodynamic wind tunnel at the UNH student wind tunnel. The set-up for the porous disk experiments is shown in Figure 5.

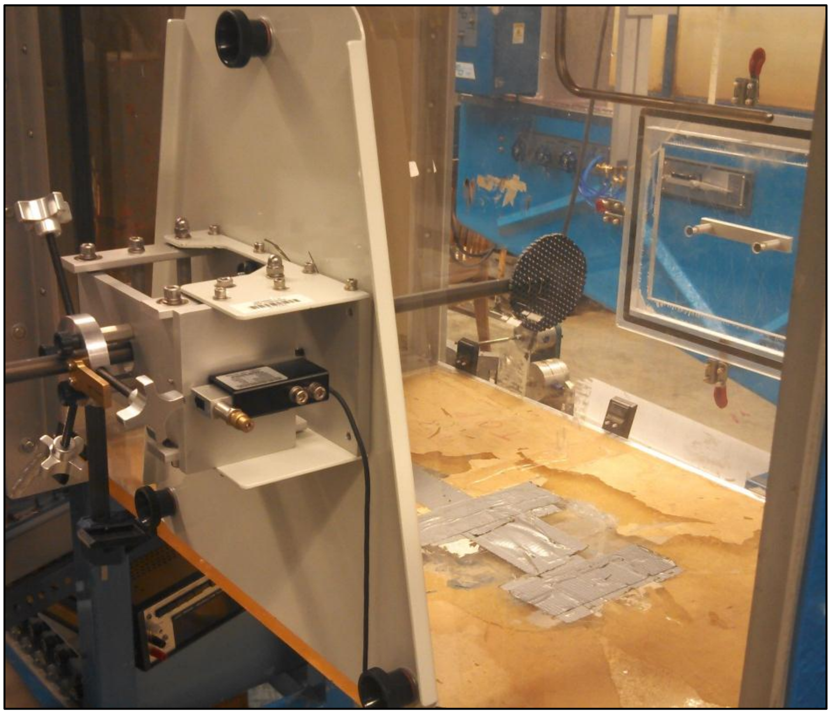

Figure 33: Experimental set-up for the porous disks in the small aerodynamic wind tunnel at UNH. A 3” diameter disk with a porosity of 0.32 is shown mounted on a sting.

The force balance used to measure the force acting on the porous disks was calibrated using a set of calibration weights. The calibration curve for the force balance is shown in Figure 6.

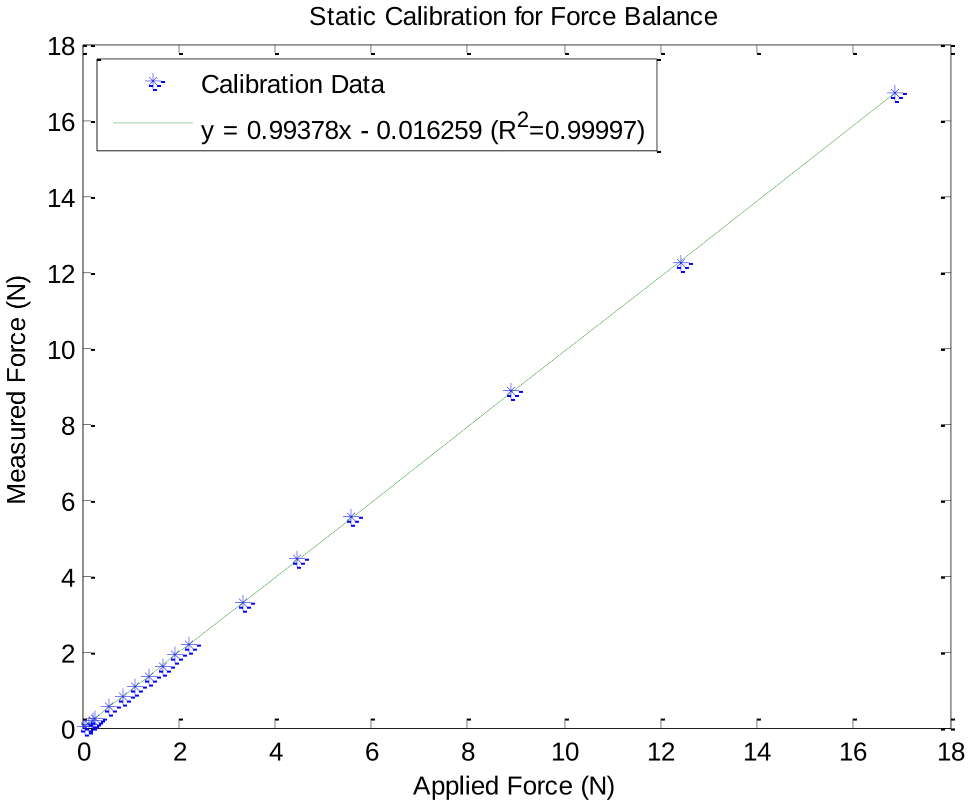

Figure 34: Calibration curve for the force balance in the UNH Student Wind Tunnel.

The calibration curve for the force balance shown in Figure 34 indicated the force balance had an offset of only 0.016 N. As this is significantly lower than the resolution of the strain gage load cell, this error can be neglected. The porous disks were tested at wind speeds varying from approximately 4-30 m/s.

Data was acquired "by hand" by visually reading a water column height on a manometer bank connected to the pitot static tube (to calculate test section velocity) and by visually reading a drag force value on a digital read-out of the force balance. Several "random samples" – readings taken at different times were averaged to approximate a mean value. However, due to this manual data acquisition a certain amount of scatter exits in the data.

Results and Discussion

For an initial comparison to an actual rotor with three blades, a 3-bladed RC plane propeller with 10” diameter was purchased, attached to a small unloaded 12 V DC motor, and run through the same tests as the porous disks. It is important to note, due to the dimensions of the test section, the data was corrected for blockage effects. The velocity measurements taken were adjusted using

$$V_{corr} = V_o\left(1 + .25\frac{A_{obj}}{A_{test}}\right), \tag{11}$$

where V_o is the un-corrected velocity, A_{obj} is the area of the object being tested, and A_{test} is the cross sectional area of the test section. Along with the blockage corrections, the drag of the exposed rod was experimentally determined and subtracted from the total disk drag. The results of the porous disks and RC plane propeller drag/thrust measurements are shown in Figures 7-9.

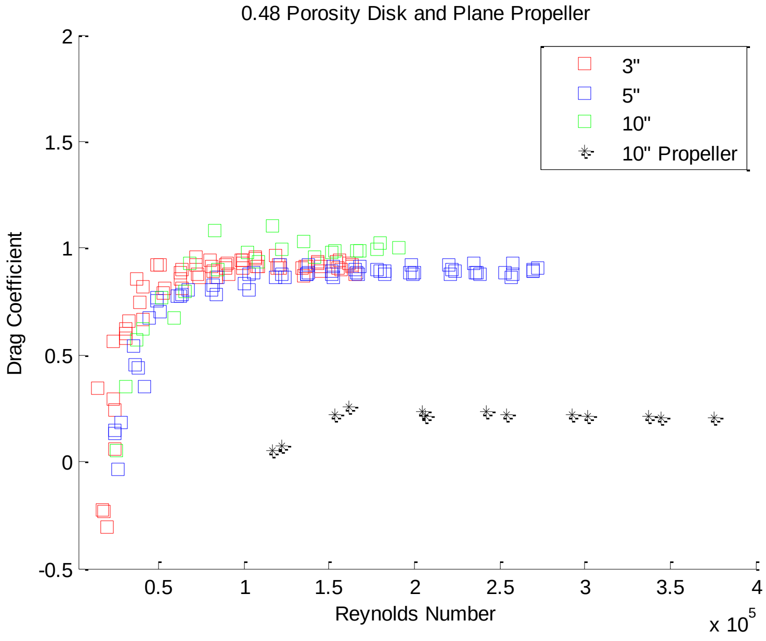

Figure 35: Drag coefficients vs. Reynolds number for 0.48 porous disk and plane propeller.

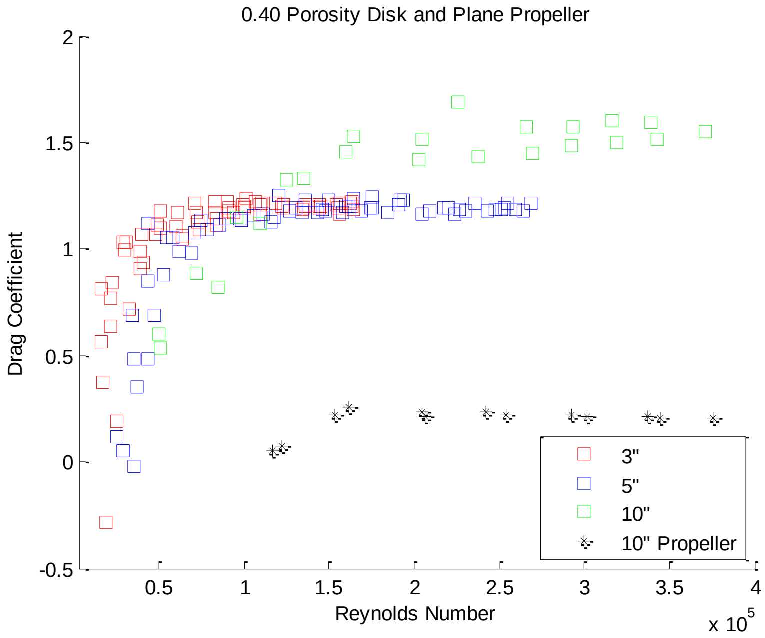

Figure 36: Drag coefficients vs. Reynolds number for 0.40 porous disk and plane propeller.

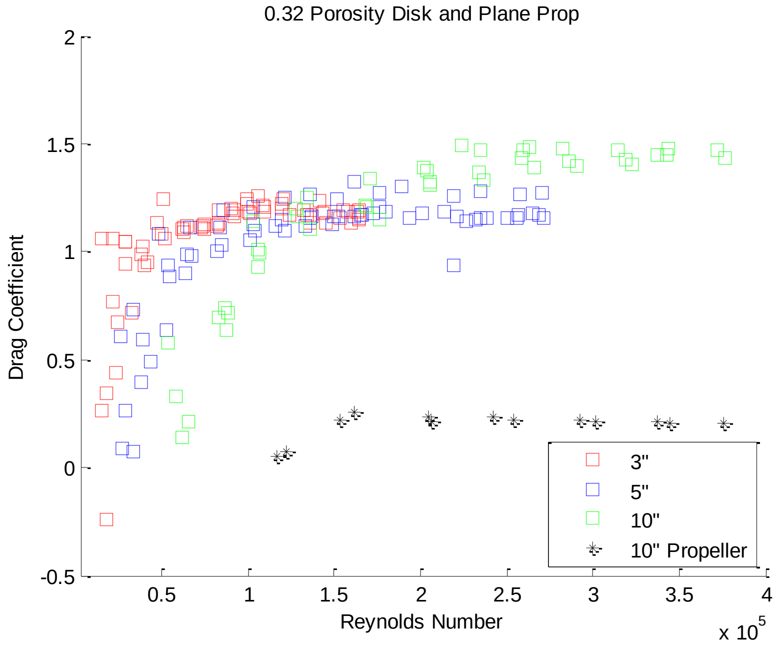

Figure 37: Drag coefficients vs. Reynolds number for 0.32 porous disk and plane propeller.

It is important to note, despite corrections for blockage, the effects of blockage in the test section can be seen in Figures 7-9. This can easily be seen for both the 0.32 and 0.40 porosity disks, where the

10” porous disk shows a significantly higher drag coefficient than the 3” and 5” disks. In theory, the drag coefficient should be independent of disk diameter and only depend on Reynolds number It can be seen that the drag coefficient becomes independent of Reynolds number above Re_D~80,000.The drag coefficient data for the RC plane propeller shown in all three porous disk results indicates the drag coefficient of the propeller is approximately 0.25. This drag coefficient is significantly lower than the data shown in Figure 4 for the full scale turbine. The data shown in Figure 4 does experience a drag coefficient at or below that of the RC propeller at high wind speeds. However, the target wind speed for later experimentation is ~7 m/s (due to wind tunnel restrictions) which would indicate a desired thrust coefficient of ~0.8. The difference between the thrust coefficient of the propeller and the full scale turbine is most likely a result of the intended purpose of the propeller, as it was not designed to extract energy from the wind. Note that if the propeller rotates in the direction of the leading edge of the blade profiles, the camber is oriented in the wrong direction. The results from the porous disk drag experiments show that the disks with a porosity of 0.48 were close to the target drag coefficient of 0.8 with an average C_D~0.85 for the 3” and 5” disks for Reynolds numbers based on diameter above10^5. A slightly higher porosity material may be necessary to achieve the target drag coefficient of 0.8.

Flow Physics Facility Test Plan

Measurement Devices

Force Balance: Model wind turbine, attached to 2 linear sliders presses against a 5lbf Omega LCEB-5 force transducer. The transducer is powered with an excitation voltage of 5V and the output is connected to an amplifier. The output of the amplifier is connected to an oscilloscope for the voltage to be read and recorded to a data acquisition system for later analysis.

24 V DC Motor: A wind turbine rotor assembly will be attached to the shaft of an Anaheim Automation 24V DC brushless motor. Each motor will be wired in series with identical resistances, with their output being read to and saved to a data acquisition system for later analysis.

With each motor under the same load, they would all have equal power extraction and RPM if they were all subjected to the same free stream velocity. In our case, with the turbines set up in a pre-determined array, it will be possible to measure a drop in power extraction from the motors farther back in the array due to the decrease in the wind velocity they are encountering.

Pitot-Tube: The wind velocity at hub height of the model turbines will be found using a pitot-tube system that digitally outputs to a data acquisition system to be saved for later analysis.

In Flow Physics Facility

1. Obtain power curve and thrust for a single wind turbine, compare to small wind tunnel results.
   Place 1 model wind turbine attached to force balance in wind tunnel.
   - Using output of force transducer measure drag force acting on wind turbine
   - Using output of 24V DC motor, measure power extraction of turbine
   - Go through a range of velocities (as allowed by tunnel operating conditions), maybe 4, 5, 6, 7 m/s (higher if early evening or weekend, and once honeycomb is fixed)

2. Obtain power curve and thrust for a single wind turbine in turbulent boundary layer of FPF
   Place 1 model wind turbine attached to force balance in wind tunnel.
   - Using output of force transducer measure drag force acting on wind turbine
   - Using output of 24V DC motor, measure power extraction of turbine
   - Go through a range of velocities (as allowed by tunnel operating conditions), maybe 4, 5, 6, 7 m/s (higher if early evening or weekend, and once honeycomb is fixed)

3. Place 1 model wind turbine in wind tunnel. Starting 6 diameters (1m) upstream of 1st turbine place another. Place another turbine attached to the force balance 4 diameters

(1m) upstream of the 2nd turbine, so there is an equally spaced 3x1 array of turbines. At the same time and in increments of 1 diameter (1m) move the 2nd and 3rd turbine upstream of the 1st, making sure to keep all turbines equidistant of each other. At each of these increments measure the following data:

- Using the output of the force balance, measure the drag force acting on the rear wind turbine.
- Using output of the 24V DC motors, measure the power extraction of the 3 turbines.

Material List

Specs for hardware used in construction of turbines

Threaded rods (8)

Steel drive shaft -Made of 1566 steel, these shafts are stronger than stainless steel shafts but are less corrosion resistant. They are unhardened for easier machining. Rockwell hardness is C25. Ends arebeveled.

Diameter = 3/8”
Length = 163mm
Bottom thread = 25mm
Top thread = 13mm

Balance threaded rod (1)

Length = 140mm

Baseplates (8)

Unpolished (Cold Drawn)
Material is 1018 carbon steel
Yield Strength: 54,000 psi
Hardness: Medium (Rockwell B70)
Can be surface hardened to Rockwell C60
Meet ASTM A108
Dimensions= ½”x6”x6”

Balance baseplate(1)

Aluminum=?
Dimensions= ½”x6”x10.5”

Sliding plate(1)

Aluminum=?
Dimensions= 3/8”x3”x3.5”
Sliders gap = 1.684”

L-bracket(8)

Width= 1.6”
Thickness= 3/16”
Leg 1= 1”
Leg 2= 1.5”

Motor spec sheet

Rated Torque (oz-in)	18
Rated Voltage (V)	24
Rated Power (Watts)	52
Rated Speed (rpm)	4000
Torque Constant (oz-in/A)	5.00
Back EMF Voltage (V/kRPM)	3.72
Winding Resistance (ohm)	0.80
Line-to-Line Inductance (mH)	1.20
Rotor Inertia (oz-in-sec^2)	0.0000000
Length (in)	2.4
Shaft	Double
Weight (lbs)	0.94
Winding Type	Delta, 8 Poles
Hall Effect Angle	120 Degree Electrical Angle
Shaft Run Out	0.025mm
Radial Play:	0.02mm@450g
End Play	0.08mm@450g
Max. Radial Force	28N 20mm from the Flange
Max. Axial Force	10N
Insulation Class	Class B
Dielectric Strength:	500VDC for one Minute
Insulation Resistance	100MOhm, 500VDC

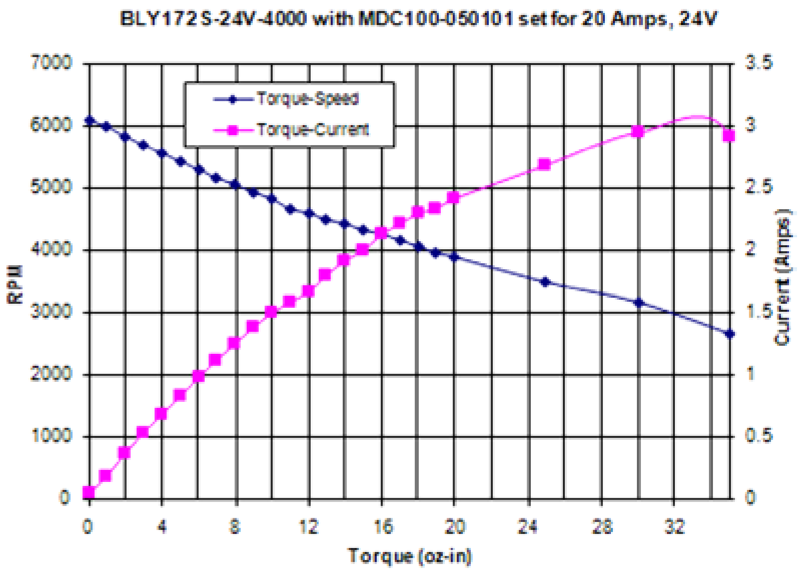

Linear slider (2)

Low Profile

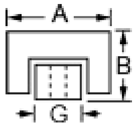

End View

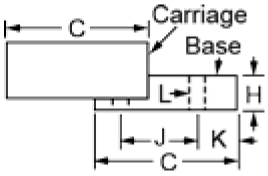

Side View

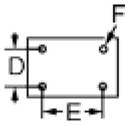

Style 1 Carriage
Mounting Holes
(Top View)

Stroke Length (in)	2
Dynamic Load Capability (lbs)	12
Wd. (A) (in)	0.56
Ht. (B) (in)	0.32
Lg. (in)	3.6
Ctr.-to-Ctr. Mounting holes (D) (in)	0.22
(E) (in)	2.63
Screw Size (F)	2-56
Dp. (in)	0.107
Base (wd.) (G) (in)	0.25
Base (Ht) (H) (in)	0.19